Optical Engineering

SPIEDigitalLibrary.org/oe

Shack-Hartmann wavefront sensor image analysis: a comparison of centroiding methods and image-processing techniques

Alice M. Nightingale
Stanislav Gordeyev

SPIE

Shack-Hartmann wavefront sensor image analysis: a comparison of centroiding methods and image-processing techniques

Alice M. Nightingale
Stanislav Gordeyev
University of Notre Dame
Institute for Flow Physics and Control
Hessert Laboratory, Building #66
Notre Dame, Indiana 46556
E-mail: aduesing@nd.edu

Abstract. Spot estimation accuracy of Shack-Hartmann images and its impact on Airborne Aero-Optic Laboratory (AAOL) wavefront statistics are addressed. A study is conducted of an individual spot simulated using a double sinc function under varying degrees of additive non-zero mean Gaussian noise within a 15×15 pixel area-of-interest. The focus of this paper is two-fold. First, the accuracy of four existing centroiding methods including first moment, convolution, Gaussian, and weighted first moment are compared. It is found that the weighted first moment centroid most accurately estimates spot centers but requires significantly more computational time with respect to the first moment method. Second, three image-processing techniques, including gamma correction, thresholding, and windowing, are analyzed to determine their influence on each centroiding method's spot estimation accuracy. A fourth order gamma correction significantly reduces spot estimation error for three centroiding methods. The key result is that the accuracy of the first moment centroid with an applied gamma correction is comparable to the weighted first moment without the computational burden. Finally, the first moment centroid with gamma correction and weighted first moment centroid are applied to AAOL flight data. Wavefront statistics are computed and compared to the commonly used first moment centroid. [DOI: 10.1117/1.OE.52.7.071413]

Subject terms: image-processing; wavefront sensors; signal-to-noise ratio; wavefronts; optics.

Paper 121439SS received Oct. 2, 2012; revised manuscript received Feb. 5, 2013; accepted for publication Feb. 6, 2013; published online Mar. 7, 2013.

1 Introduction

Aircraft induced aberrations, referred to as aero-optics, are known to severely limit a directed energy system's field of regard.[1,2] Optical turrets, which house these airborne lasers, create complex flows on and around the hemisphere-on-cylinder imparting aberrations on a beam as it projects through the flow.[3,4] With the increased use of shorter wavelength lasers, the index-of-refraction variations related to the low-pressure regions in the near-field of a turret significantly reduce system performance by imposing optical aberrations to the laser even in low Mach number flights.[1] Wind-tunnel and in-flight testing are used to study the role of aero-optic effects on system performance and to develop different mitigation techniques.

An accurate characterization of the aero-optic environment requires accurate wavefront measurements. The Shack-Hartmann wavefront sensor is an optical instrument commonly used in adaptive-optic systems to approximate the optical wavefront of an incident light beam. The sensor was developed in the late 1960s, evolving from the Hartmann screen test.[5] It consists of an array of lenses positioned in front of a photon detector which partitions the incoming beam into a grid of subapertures creating an array of spots focused on the face of the sensor. The sensor converts light, or intensity, into a proportional voltage signal which is used to compute local tilt, or wavefront slope. The set of wavefront slope measurements may then be integrated to reconstruct the instantaneous optical wavefront, or irradiance pattern assuming that the spatial pattern partitioning the incoming light sufficiently resolves the relevant spatial frequencies of the aberrated wavefront.

Notre Dame's Airborne Aero-Optics Laboratory (AAOL) is a test bed designed to acquire in-flight aero-optic measurements caused by turbulent flow on and around an aircraft turret. The AAOL captures wavefronts using a high-speed Phantom v711 Shack-Hartmann wavefront sensor with frame rates up to 20 kHz. A spatial resolution of 32×32 lenslets is most often used during testing to maximize the frame rate capabilities of the camera.[6] As described above, the incoming light beam is partitioned through these lenslets into an array of subapertures each consisting of approximately 15×15 pixels. On average the spot size within each subaperture has a full-width at half-maximum (FWHM) of between 3 and 4 pixels. A 15×15 pixel subaperture grid containing a single spot whose FWHM was approximately 3.5 pixels was simulated for this paper in an effort to study subaperture conditions commonly captured by the AAOL. Background light levels and noise were also simulated over a range of values including those commonly found in the AAOL data as will be further discussed in the next section.

The accuracy of the reconstructed wavefront is largely dependent upon the determination of the spot centers, commonly referred to as "centroiding." The first moment calculation, defined as

$$x_c' = \frac{\sum_i^{N_i}\sum_j^{N_j} x_i I_{i,j}}{\sum_i^{N_i}\sum_j^{N_j} I_{i,j}} \quad \text{and} \quad y_c' = \frac{\sum_i^{N_i}\sum_j^{N_j} y_j I_{i,j}}{\sum_i^{N_i}\sum_j^{N_j} I_{i,j}}, \tag{1}$$

is the prevailing method used to locate the center of each spot, (x_c', y_c') within an area-of-interest (AOI), and has been the chosen method used to process the AAOL data. This method provides a robust centroid calculation with minimal computational time. However, since the first moment centroid is an intensity based method, increased noise levels result in significant spot estimation error. This paper investigates four existing centroiding methods, including the first moment centroid, and the effect of applying three different image processing techniques prior to spot estimation. Accuracy is examined by comparing each estimate of the spot center to the simulated spot's true center. Computational times for each method are presented. The comparison is meant to aid the reader in selecting the most suitable centroiding method for a particular data processing application.

Three different forms of image processing techniques are explored including a gamma correction, thresholding, and windowing. The gamma correction is a simple means of enhancing the image's bright pixels while reducing noise using a power-law. Thresholding is another common technique used to reduce noise by raising the relative "floor" of the image and is used currently to process the AAOL data. A percent threshold based on the maximum pixel intensity is examined in this paper. Windowing similarly removes noise by isolating the relevant or bright pixels, within the image. For the studies shown here, the window is centered at the pixel with the maximum intensity.

The following section outlines the simulation approach used to study each of the four different centroiding methods as well as image processing techniques. Simulations are performed given a spot within a single AOI in order to compare centroiding error between each of the methods investigated. These results are then used to select two of the most accurate centroiding techniques, in addition to the method currently being used to process the AAOL data, which are applied to two different sets of AAOL flight data. Wavefront statistics are computed and presented and a further comparison between methods is discussed.

2 Simulation Approach

A double sinc function, defined as

$$I(x,y) = I_o\left[\frac{\sin(x-x_o)}{\omega_x x}\frac{\sin(y-y_o)}{\omega_y y}\right]^2, \tag{2}$$

where x_o and y_o represents the relative spot center and ω_x and ω_y are the scaling constants, is simulated on a 1500×1500 grid as pictured in Fig. 1 (note: the range of intensity values shown in Fig. 1 has been modified slightly to enhance the outer lobes for visual purposes only). This type of function most closely resembles the rectangular spot pattern created by each square lenslet which is captured by the AAOL wavefront sensor. Figure 2 shows a typical AOI taken from an AAOL Wavefront image. As shown, the spot appears to be rectangular with four outer lobes similar to a double since function. The AOI shown in Fig. 2 is made up of a 15×15 pixel area, a size typically found within the AAOL data sets. As such, the simulated image is partitioned into a similar 15×15 pixel AOI [refer to Fig. 3(a)] by computing the mean intensity within each pixel area corresponding to a 100 by 100 set of points from the original image (Fig. 1). Finally, additive Gaussian noise with a nonzero mean is applied to the simulated 15×15 pixel image [Fig. 3(b)]. A range of mean and variance values, referred to in this paper as mean noise level and noise variance, are studied. Figure 3(a) shows a simulated spot centered at (0,0) within a 15×15 pixel AOI before applying any noise. Figure 3(b) shows the same simulated spot after applying additive Gaussian noise given a mean noise level of 0.025 and a noise variance of 0.001. For the results reported in this paper, a double since function resulting in a FWHM of approximately 3.5 was simulated. Each image was normalized to create a maximum brightness value of 1. The spot size and AOI grid size were selected based on typical sizes measured by the high-speed Phantom Shack-Hartmann

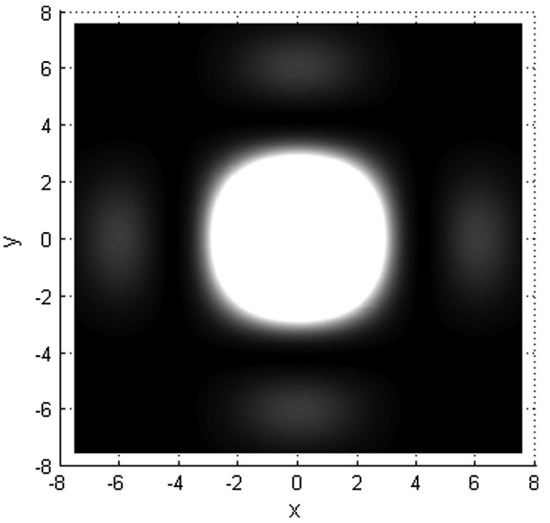

Fig. 1 Simulated double sinc pattern on a 1500×1500 grid with an amplitude of 1 and a full-width half maximum of approximately 3.5.

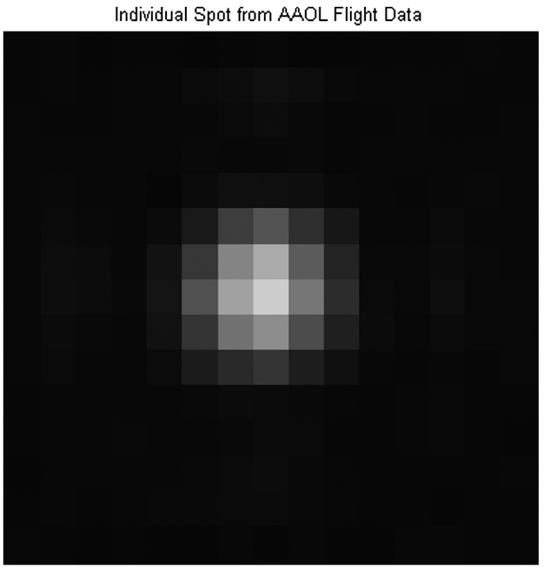

Fig. 2 Single 15×15 pixel subaperture grid from a Shack-Hartmann sensor image captured within a set of AAOL data.

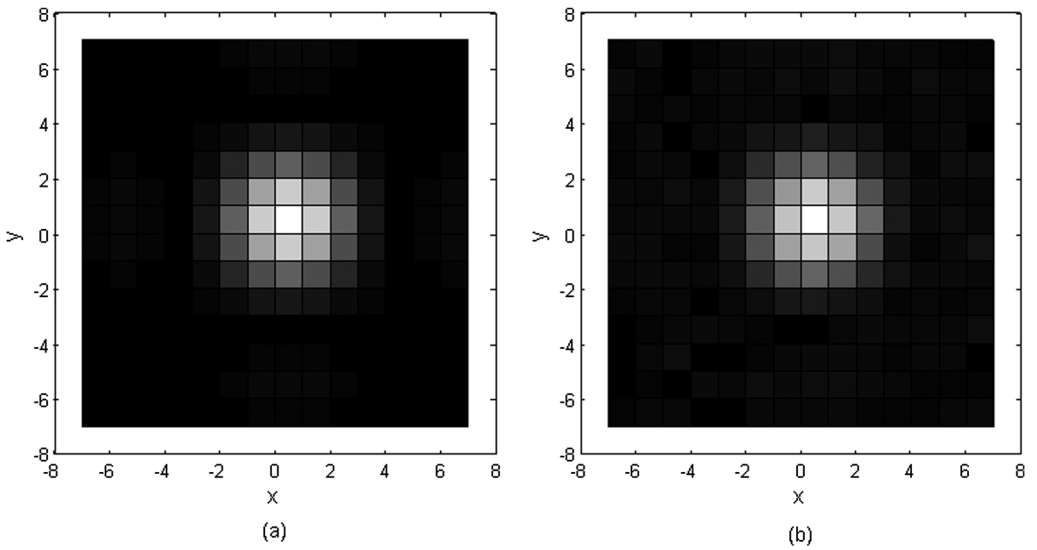

Fig. 3 Simulated 15×15 pixel AOI created from the double sinc pattern shown in Fig. 1 (a) with no noise and (b) with additive Gaussian noise given a mean of 0.025 and variance of 0.001.

wavefront sensor used on the AAOL at Notre Dame for in-flight testing.[7,8]

Varying noise levels are applied during each simulation in order to study its effect on the centroid calculations. The amount of noise is quantified by a signal to noise ratio (SNR), defined as the ratio of the bounded signal's range to the standard deviation, σ_N, of background noise,

$$\mathrm{SNR} = 20 \log_{10}\left(\frac{s_{\max} - s_{\min}}{\sigma_N}\right), \tag{3}$$

where $s_{\max}$ and $s_{\min}$ represent the signal's maximum and minimum values, respectively, for a given simulation.[9] Additive Gaussian noise is applied to the pixelated image at mean noise levels of 0.005, 0.01, 0.025, 0.05, 0.1, and 0.2, while the noise variance ranges from 1e-20 to 1e-1. These noise variance levels correspond to SNRs ranging from approximately 10 to 200, where SNRs above 80 indicate low noise levels and SNRs below 30 represent high noise levels or poor sensor imaging. At SNRs of 10 or more the spot becomes virtually indiscernible. Mean noise levels of 0.05 (corresponding to 5% of the image maximum) and above represent large amounts of background ambient light levels and/or significant amounts of dark current on the sensor.

Mean noise and variance levels were selected based upon values commonly measured by the AAOL. Background noise was estimated for several sets of AAOL flight data by computing the mean and variance of four corner regions on each Shack-Hartmann wavefront sensor image as depicted in Fig. 4. Mean noise levels were found to range from approximately 0.01 to 0.03 while the SNRs ranged from approximately 25 to 55 for the data studied. Simulation results reported throughout this paper focus on these noise levels; however, it should be noted that centroiding error was found to scale with mean noise level. The experimental noise values were computed after normalizing the AAOL images from 0 to 1.

The primary purpose of this paper is to investigate four different existing centroiding methods along with a few image processing techniques in an effort to compare

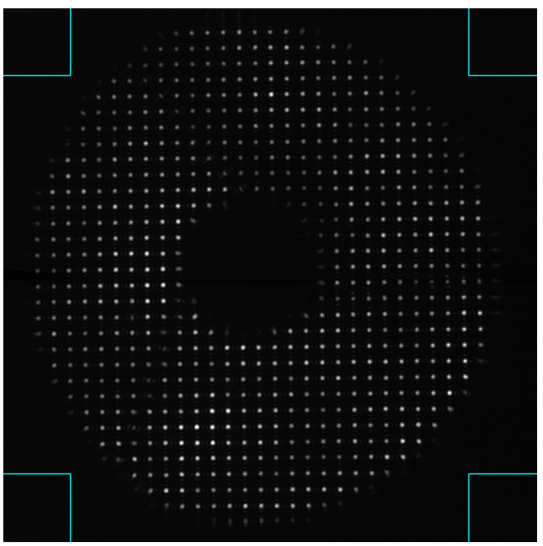

Fig. 4 Shack-Harmann wavefront sensor image from a set of AAOL data.

accuracy and computational time. For each simulation, the spot position, or spot center, is estimated using each of the four centroiding methods detailed below within a simulated AOI. The absolute centroiding error (ACE) referred to in this paper is defined as

$$\mathrm{ACE} = \sqrt{(x_c - x_c')^2 + (y_c - y_c')^2}, \tag{4}$$

where (x_c, y_c) represents the position of the actual spot center and (x_c', y_c') represents the estimated position based on one of the four centroiding methods. The ACE is computed based on each method for a given simulation. An average ACE value is then determined from a set of 500 randomly simulated images given a specified mean and variance noise level.

In addition to the commonly used first moment centroid defined above in Eq. (1), three more existing methods are

compared throughout this paper: a convolution centroid, a Gaussian centroid, and a weighted first moment centroid. The convolution centroid is obtained by first performing a discrete two-dimensional convolution using the Matlab command *conv2* with the shape parameter "same." Once the 15×15 pixel matrix (simulated AOI) is convolved with another 15×15 matrix containing a predetermined Gaussian shape, the spot center is estimated using the first moment calculation defined by Eq. (1). A Gaussian centroid is also examined using an over determined weighted regression model.[10] As described,[10] a circular Gaussian function, without the influence of noise, may be transformed into the following linear equation using the logarithm

$$c_1 x_i + c_2 y_j + c_3 \ln(I_{i,j}) + c_4 = (x_i^2 + y_j^2), \tag{5}$$

where c_1, c_2, c_3, and c_4 are unknown coefficients defined as follows:

$$c_1 = 2x_c' \tag{6}$$

$$c_2 = 2y_c' \tag{7}$$

$$c_3 = -2\sigma_w^2 \tag{8}$$

$$c_3 = -2\sigma_w^2 \ln(A) - x_c'^2 - y_c'^2. \tag{9}$$

As long as there are more than four pixels with the simulated AOI, the circular Gaussian approximation results in an over determined set of linear equations which may be solved using a linear least-squares regression.[10] The backslash (/) is used in Matlab to obtain the solution to the over determined set of equations in the least-squares sense for the results shown in this paper. An iteratively weighted first moment centroid[11] is the fourth method examined. It uses a weighting function, $W(x, y)$, with a Gaussian form whose central position iteratively adjusts based on the previous iteration's weighted first moment calculation,

$$x_c' = \frac{\sum_i^{N_i} \sum_j^{N_j} x_i I_{i,j} w_{i,j}}{\sum_i^{N_i} \sum_j^{N_j} I_{i,j} w_{i,j}} \quad \text{and} \quad y_c' = \frac{\sum_i^{N_i} \sum_j^{N_j} y_j I_{i,j} w_{i,j}}{\sum_i^{N_i} \sum_j^{N_j} I_{i,j} w_{i,j}}. \tag{10}$$

The center location of the weighting function for the first iteration is obtained based on an initial first moment calculation [Eq. (1)] and the Gaussian spread (or width), σ_w, is estimated based on an estimation of the spots' FWHM, where $\sigma_w \approx (\text{FWHM}/2.3548)$. The newly computed spot center becomes the weighting functions center for the next iteration. This process is repeated until the computed spot positions in both the x- and y-directions converge to within 0.001 pixels of the previous iteration. Sections 3.1 and 3.2 present simulation results based on these four

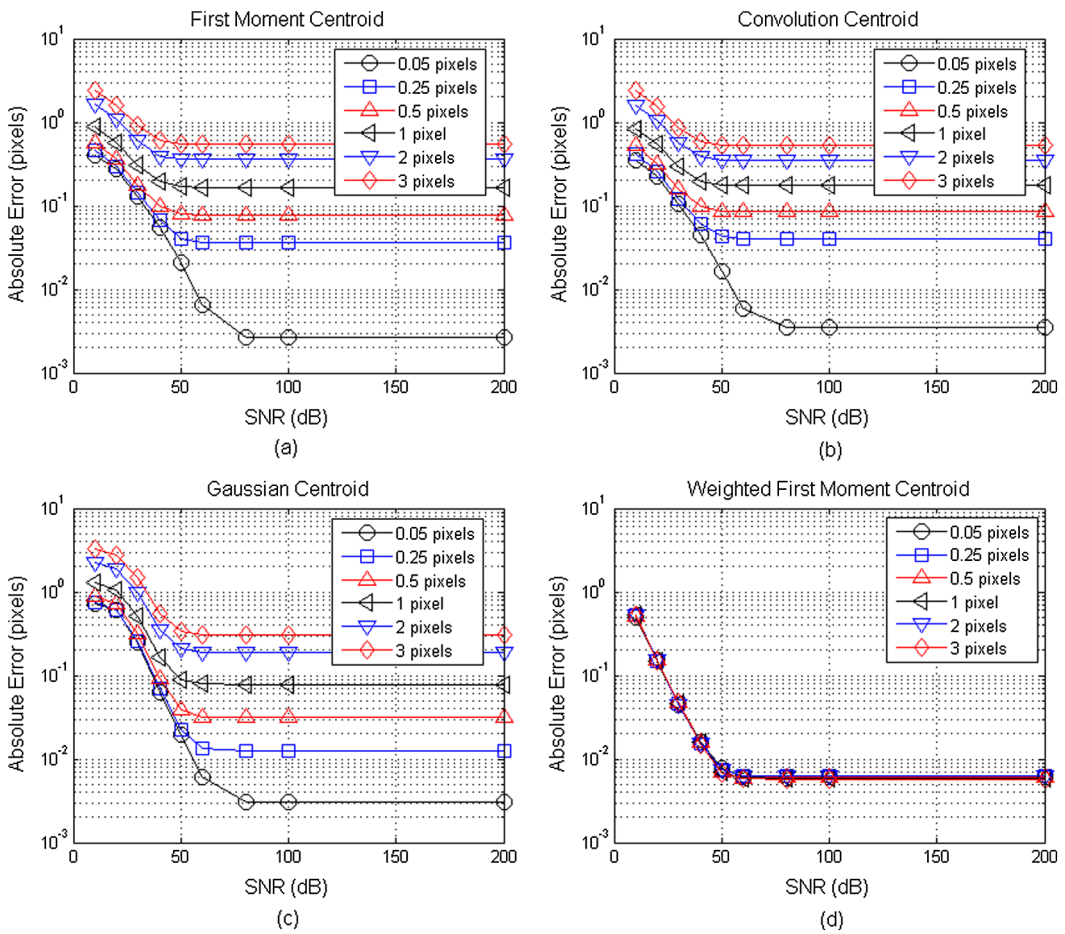

Fig. 5 Absolute error (pixels) versus SNR (dB) given six different spot positions with respect to the center of the AOI with a mean noise level of 0.01. Error was computed based on four centroiding methods: (a) first moment, (b) convolution, (c) Gaussian, and (d) weighted first moment.

centroiding methods for a spot fully within the AOI boundary and partially out of the AOI boundary, respectively. Computational times for all four methods are addressed in Sec. 3.3.

3 Centroid Estimation Results

3.1 *Spot Fully within AOI Boundary*

The first set of results shown below present a comparison between the four centroiding methods described above for spot positions between 0 and 3 pixels from the AOI's center. For each position presented in this section the entire spot remains within the AOI. The ACE, or absolute error, defined by Eq. (4), is plotted against SNRs, where large SNRs correspond to small amounts of image noise and vice versa. Figures 5, 6, and 7 show absolute error (pixels) versus SNR (dB) given mean noise levels of 0.01, 0.025, and 0.05, respectively. Several other mean noise levels not shown here were also simulated and found to scale proportionally.

The first moment centroid and convolution centroid perform very similar at all mean noise levels where the absolute error decreases with increasing SNR until leveling off beyond approximately 60 dB. Both methods exhibit more error as the spot position moves farther from the center of the AOI. This is due to their intensity based calculations. As the spot moves off center in the AOI, the amount of noise on either side of the spot becomes disproportionate, inducing larger amounts of error. The Gaussian centroid performs slightly better than the first moment and convolution centroids when the mean noise level is low. However, when the mean noise level exceeds 0.01 (Figs. 6 and 7), representing a sensor with moderate to significant noise levels, the Gaussian estimate no longer outperforms the other two methods. Finally, the weighted first moment centroid provides the most accurate estimate of the spot at all mean noise levels. It also produces an absolute error seemingly independent of spot position. The iterative approach works as a filter creating an estimate that is no longer intensity based. The reduction in error though comes at a computational cost which will be discussed in a subsequent section.

3.2 *Spot Partially Outside AOI Boundary*

The next set of simulations investigates the accuracy of each centroiding method when a portion of the spot falls outside the AOI. Figure 8 displays images of four spot locations simulated for this investigation with additive nonzero mean Gaussian noise present. The AOI images were created from a double sinc function with an amplitude of 1 and FWHM of approximately 3.5. As depicted, the spot located five pixels from the AOI center [Fig. 8(a)] remains almost entirely within the AOI boundary while the spot located 8 pixels from the AOI center [Fig. 8(d)], has more than half of the spot falling outside the AOI boundary. The same four centroiding methods and their respective errors are compared below over

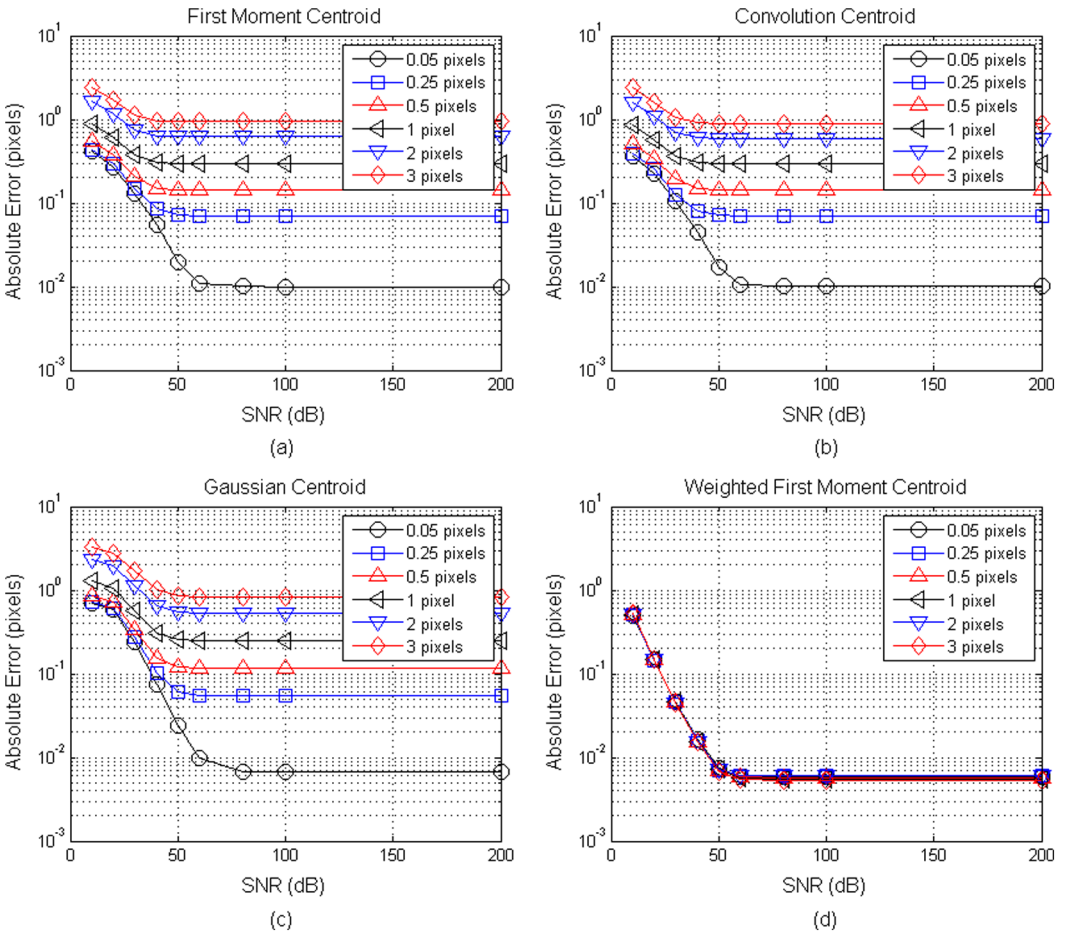

Fig. 6 Absolute error (pixels) versus SNR (dB) given six different spot positions with respect to the center of the AOI with a mean noise level of 0.025. Error was computed based on four centroiding methods: (a) first moment, (b) convolution, (c) Gaussian, and (d) weighted first moment.

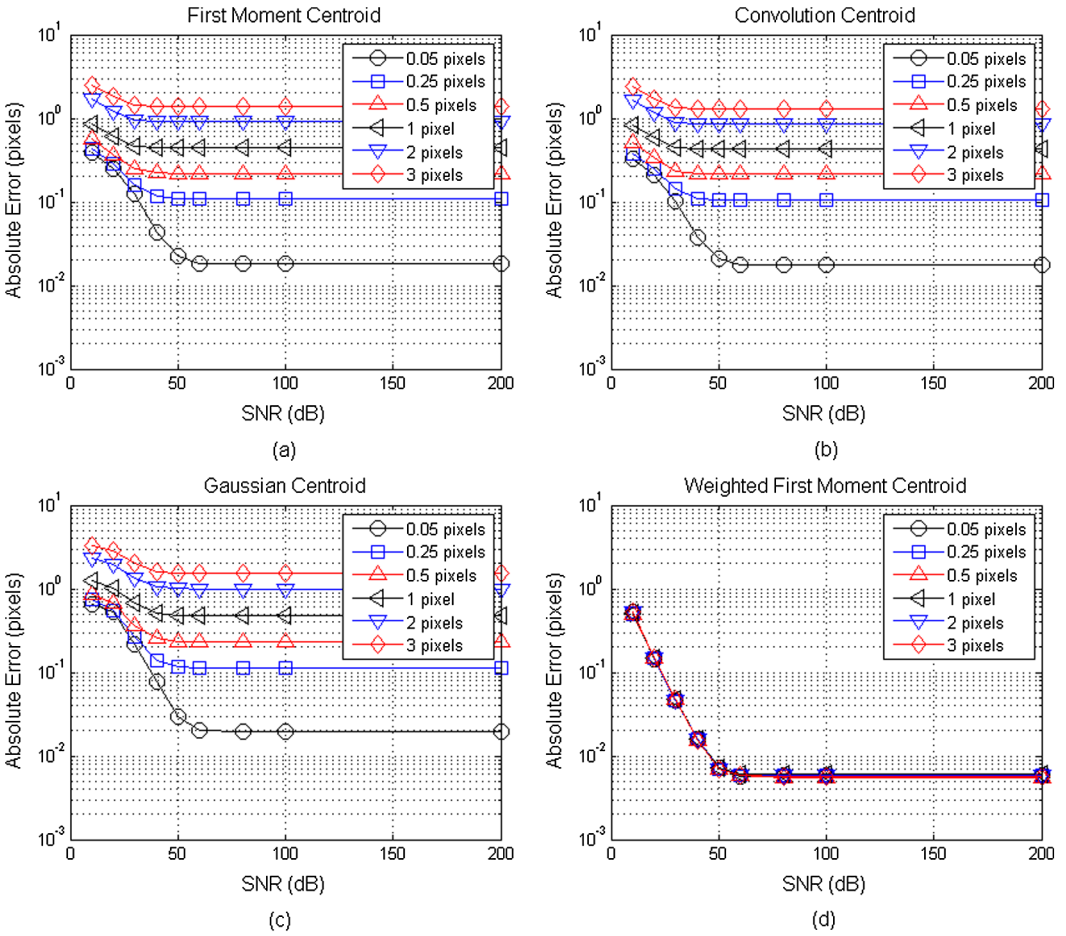

Fig. 7 Absolute error (pixels) versus SNR (dB) given six different spot positions with respect to the center of the AOI with a mean noise level of 0.05. Error was computed based on four centroiding methods: (a) first moment, (b) convolution, (c) Gaussian, and (d) weighted first moment.

a range of SNRs. Figures 9 and 10 show absolute error (pixels) versus SNR (dB) using the four centroid estimates given mean noise levels of 0.01 and 0.05, respectively.

As expected, all four methods experience more difficulty accurately estimating the spot center when a portion of the spot falls outside the AOI boundary. The first moment and convolution methods display similar trends once again and contain the most error, on the order of a pixel at the furthest positions from the AOI center. The Gaussian centroid performs slightly better at low noise levels (mean noise level of approximately 0.01) in comparison to the first moment and convolution centroids. However, as the mean noise level approaches 0.05 the performance of the Gaussian centroid behaves comparable to the first moment and convolution centroids. Overall, the weighted first moment centroid estimates the spot center with the least amount of error providing consistent results for low to moderate mean noise levels. For extremely high mean noise levels approaching 0.2, representing an extremely poor sensor or lighting conditions, the performance of the weighted first moment was found to drop slightly while still providing the most accurate estimate of the spot center.

3.3 *Computational Time*

Computational time must also be considered when selecting the optimal centroiding method for a particular application. When there are extremely large amounts of data to be processed, maintaining reasonably low computational time becomes exceedingly important. Therefore, a comparison of computational times for the four different centroiding methods described above is presented here. The simulations described throughout this paper were run using Matlab 2012b software. Computational times were recorded on a 2.6 GHz Lenovo PC with 8 GB of RAM. During each run, computational time was recorded for 500 randomly simulated images at each spot location for a given mean and variance noise level. Average computational times and standard deviations were computed for each method with respect to SNR and spot position.

Since the first three centroiding methods are noniterative, their respective computational times remain virtually constant irrespective of the noise level or spot position. While the number of iterations, and therefore computational time, for the weighted first moment centroid to reach convergence varies depending upon the amount of noise and spot position. For the results reported here, convergence is defined as the point in which two consecutive iterative steps are within 0.001 pixels of each other in both the x- and y-directions.

In order to generalize the results in this section, computational times are given as a ratio relative to the Gaussian method, which possesses the longest computational time for the results shown. Each computational time has been divided

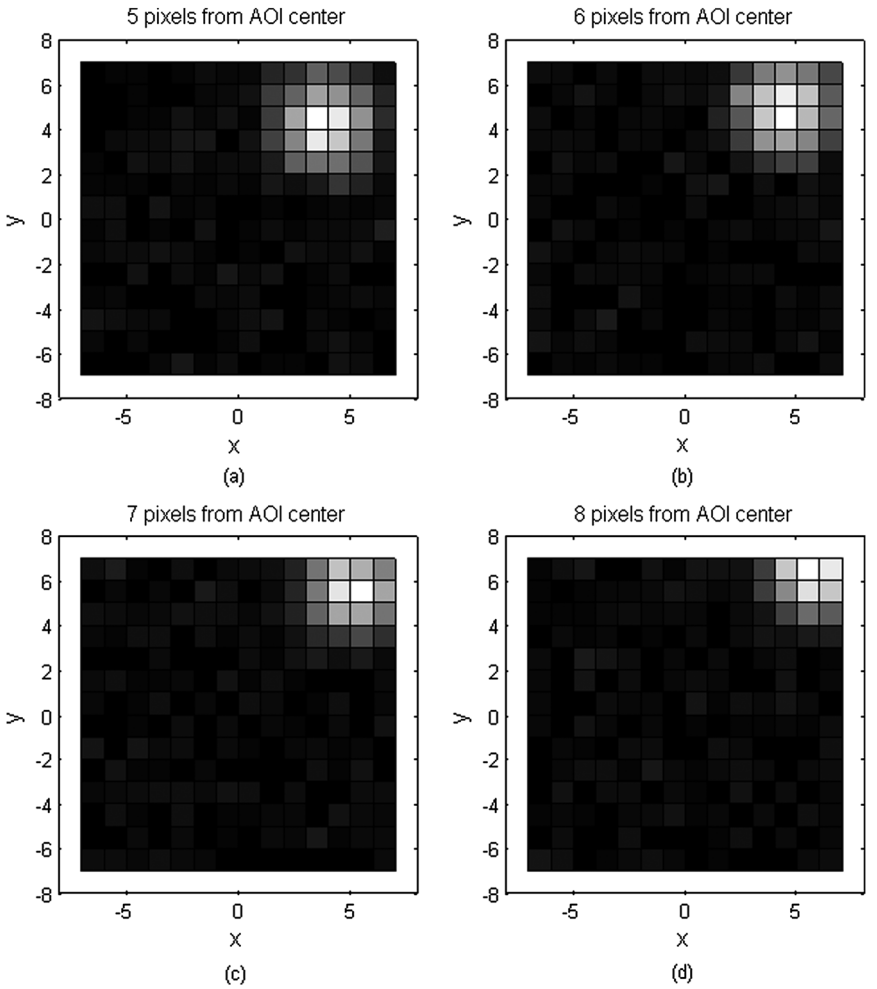

Fig. 8 Simulated image of a spot within a 15×15 pixel AOI with additive Gaussian noise given a mean noise level of 0.025 and variance of 0.001 where the spot center is located a distance of approximately (a) 5 pixels from AOI center, (b) 6 pixels from AOI center, (c) 7 pixels from AOI center, and (d) 8 pixels from AOI center.

by the Gaussian method's computational time to provide a ratio with which to compare; on average the computational time for the Gaussian method to compute a centroid takes approximately 1.2 ms for this particular computer. Figure 11 shows the resulting computational time ratios for each of the four centroiding methods recorded during a series of simulations with a mean noise level of 0.025 and a noise variance of 0.0001 (resulting in a SNR of approximately 40) where the spot center was 1 pixel from the AOI center. It is clear from this bar graph that the first moment centroid takes the least amount of computational time, less than 1/20 the time taken by the Gaussian method at a ratio of approximately 0.045. The convolution method takes approximately 1/5 as long as the Gaussian method with a ratio of approximately 0.2.

For this noise level and spot position, the weighted first moment converges onto a solution in approximately 11 iterations. For the computer described above, the first iteration of the weighted first moment takes approximately 0.153 ms while each subsequent iteration takes approximately 0.066 ms. In this case, convergence is reached in just under half the amount of time taken for the Gaussian method corresponding to a ratio of approximately 0.48. However, in comparison to the first moment centroid, 11 iterations of the weighted first moment method take approximately 10 times as long to process. Lower noise levels, as well as spot positions closer to the AOI center, require fewer iterations and therefore take less computational time as shown in Fig. 12(a) and 12(b). It should also be noted that as the SNR decreases (i.e., more noise), greater variance in computational time occurs between simulations due to the fact that there is more variation in the intensity from one randomly generated image to the next.

While the weighted first moment centroid consistently provides a more accurate estimation of the spot center, it can take significantly more computational time compared to the commonly used first moment centroid. Even a simulation only requiring three iterations for the weighted first moment centroid would take more than five times as long when compared to the commonly used first moment centroid. If minimizing computational time is highly important, a predetermined number of iterations could be used rather than using a loop within Matlab. This would save computational time by reducing the time taken for the first iteration while still benefiting from the increased accuracy of consecutive iterations. However, the image processing

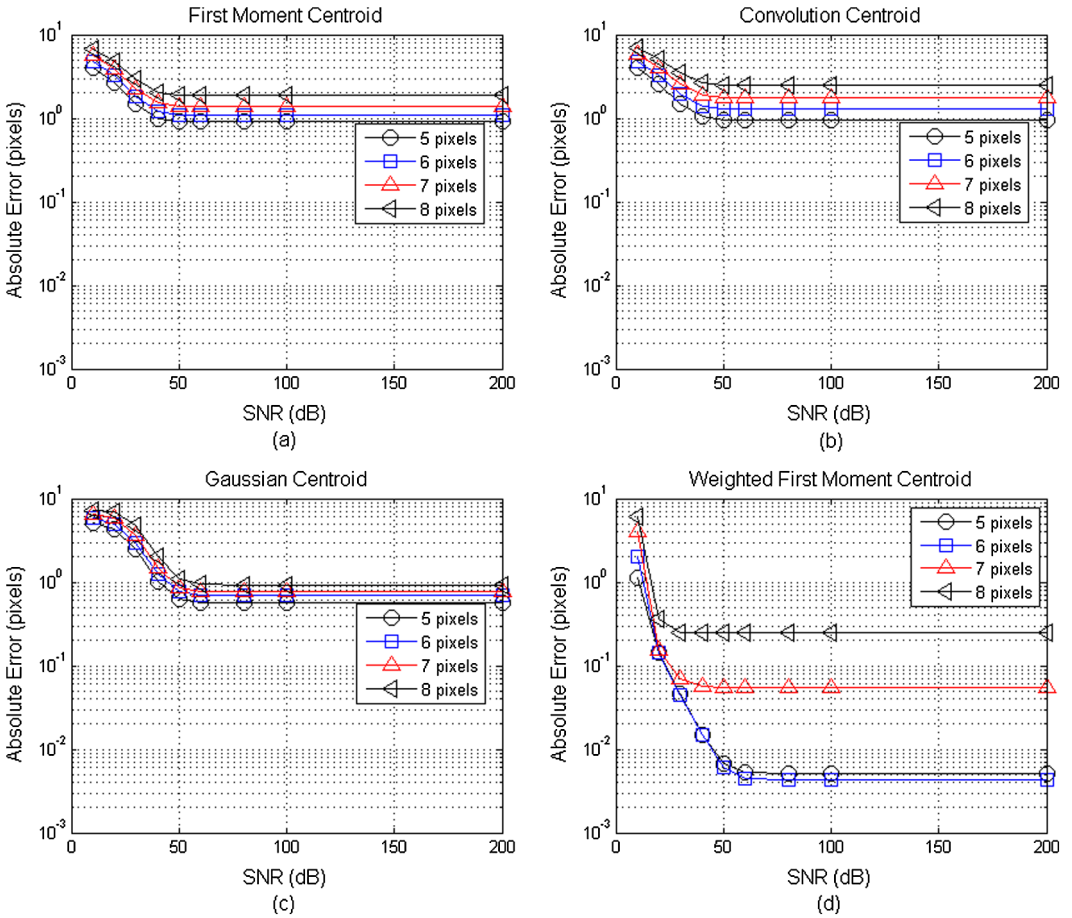

Fig. 9 Absolute error (pixels) versus SNR (dB) given the four spot positions shown above in Fig. 8 with a mean noise level of 0.01. Error was computed based on four centroiding methods: (a) first moment, (b) convolution, (c) Gaussian, and (d) weighted first moment.

techniques explored in the following section provide possibly another, less computationally demanding, means of increasing accuracy.

4 Image Preprocessing Results

4.1 *Gamma Correction*

Image enhancing is a common technique used to "modify attributes of an image to make it more suitable for a given task."[12] For this paper, two different power-law transformations, referred to as gamma corrections, are investigated: a 2nd order and a 4th order power-law. In this type of transformation, the individual pixels of the image are raised to a specified power after the image has been normalized from 0 to 1. This particular method of image enhancement produces a more focused spot while reducing the impact of background noise. Figures 13 and 14 show absolute error (pixels) versus SNR (dB) given 2nd and 4th order gamma corrections, respectively. Results are shown for each of the four centroiding methods given an initial mean noise level of 0.025.

When comparing the 2nd order gamma correction results from Fig. 13 to those shown in Fig. 6 prior to any transformation, significant improvements are observed by the first three centroiding methods. For SNRs of 30 and above, after applying the 2nd order gamma correction, the Gaussian and weighted first moment centroids perform similarly with significantly less absolute error in comparison to the first moment and convolution centroids as the spot moves away from the AOI center. However, the 4th order gamma correction results (Fig. 14) show even further reduction in absolute error for the first moment and convolution centroiding methods. Upon applying this transformation, all four methods provide similar estimates of the spot centroids. At the lowest SNR of 10 in which the noise is the greatest, the gamma correction provides the least amount of improvement which is to be expected since the spot is very difficult to discern at this noise level.

The significance of these results can be observed at SNRs between 30 and 50, typical values computed from the AAOL data. Reductions in absolute error by an order of magnitude are shown at these SNRs for the first moment centroid when a 4th order gamma correction is applied [comparing Fig. 6(a) to Fig. 14(a)]. Not only does this image processing technique improve accuracy but this type of transformation adds very little computational time in comparison to other iterative methods such as the weighted first moment centroid described in this paper. This image enhancement technique was applied to several sets of AAOL flight test data. SNRs corresponding to the individual AOIs were computed before and after applying 2nd and 4th order gamma corrections. As expected, the background noise was reduced by a factor of approximately two and almost four when raising the AOIs to the 2nd and 4th power, respectively. As a result the spot

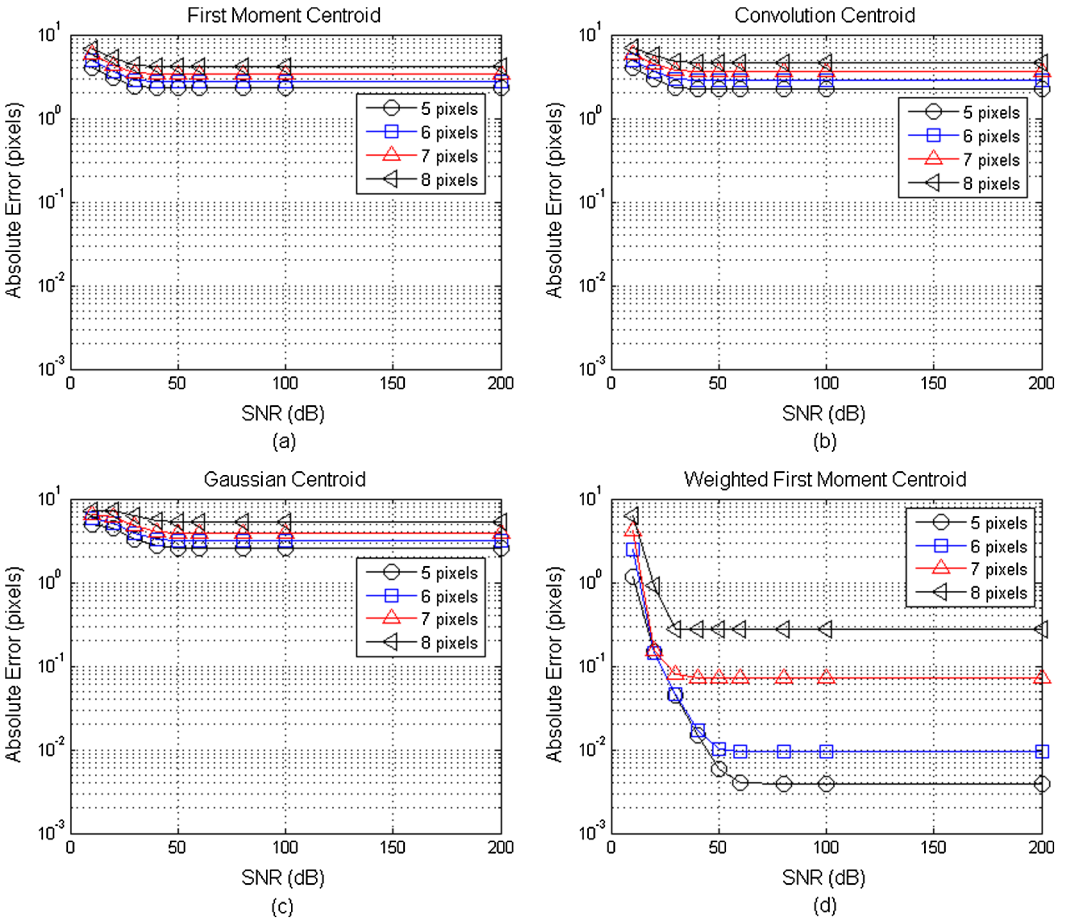

Fig. 10 Absolute error (pixels) versus SNR (dB) given the four spot positions shown above in Fig. 8 with a mean noise level of 0.05. Error was computed based on four centroiding methods: (a) first moment, (b) convolution, (c) Gaussian, and (d) weighted first moment.

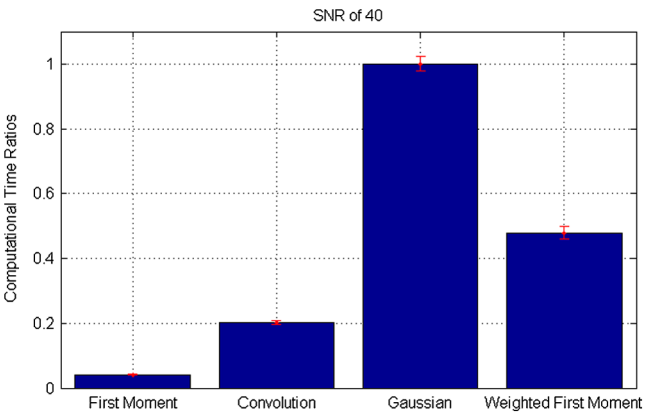

Fig. 11 Computational time ratios (relative to the Gaussian method) for the first moment centroid, convolution centroid, Gaussian centroid, and weighted first moment centroid given a simulated 15×15 pixel image with a mean noise level of 0.025 and a variance of 0.0001.

becomes more distinct, improving the accuracy of the first moment calculation. The gamma correction appears to provide a beneficial image enhancing technique without adding significant computational cost. Section 6 presents further results when this technique is applied to a series of Shack-Hartmann wavefront images taken from a set of AAOL flight data.

4.2 *Thresholding*

The second image-processing technique investigated, prior to finding the centroid, is called thresholding. A percent threshold based on the maximum intensity of the image is initially subtracted from the pixels after which all negative values are set equal to zero. This process raises the floor of the image with the goal of removing background noise. Percent threshold values between 0% and 35% are studied. Figure 15 shows absolute error (pixels) versus percent threshold given a mean noise level of approximately 0.025 for each of the four centroiding methods described throughout this paper. Results are shown for several different spot positions with respect to the AOI center given two different SNRs. As shown in Fig. 15, there appears to exist an optimal range of thresholding values for the first moment, convolution, and Gaussian centroids. For SNRs of 50 or more, a minimum 5% threshold creates significant improvement in spot center estimation. As the SNR decreases (i.e., noise variance increases), the minimum percent threshold needed to produce the optimal results increases. Thresholding becomes less effective with increased noise levels. Increasing the mean noise level also requires the use of higher percent thresholds.

While thresholding does not appear to improve the accuracy of the weighted first moment method, it does reduce its computational time. The number of iterations necessary for the weighted first moment method to reach convergence

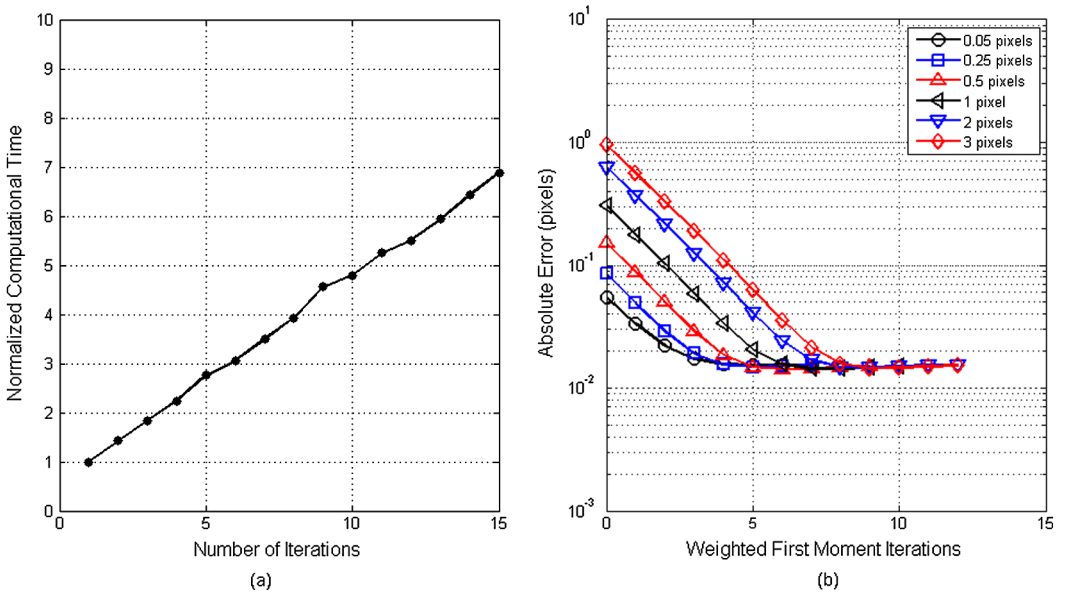

Fig. 12 (a) Computational time normalized by the time taken for the first iteration versus number of iterations for the weighted first moment centroiding method and (b) absolute error (pixels) versus number of iterations taken to reach convergence given six different spot locations measured from the AOI center.

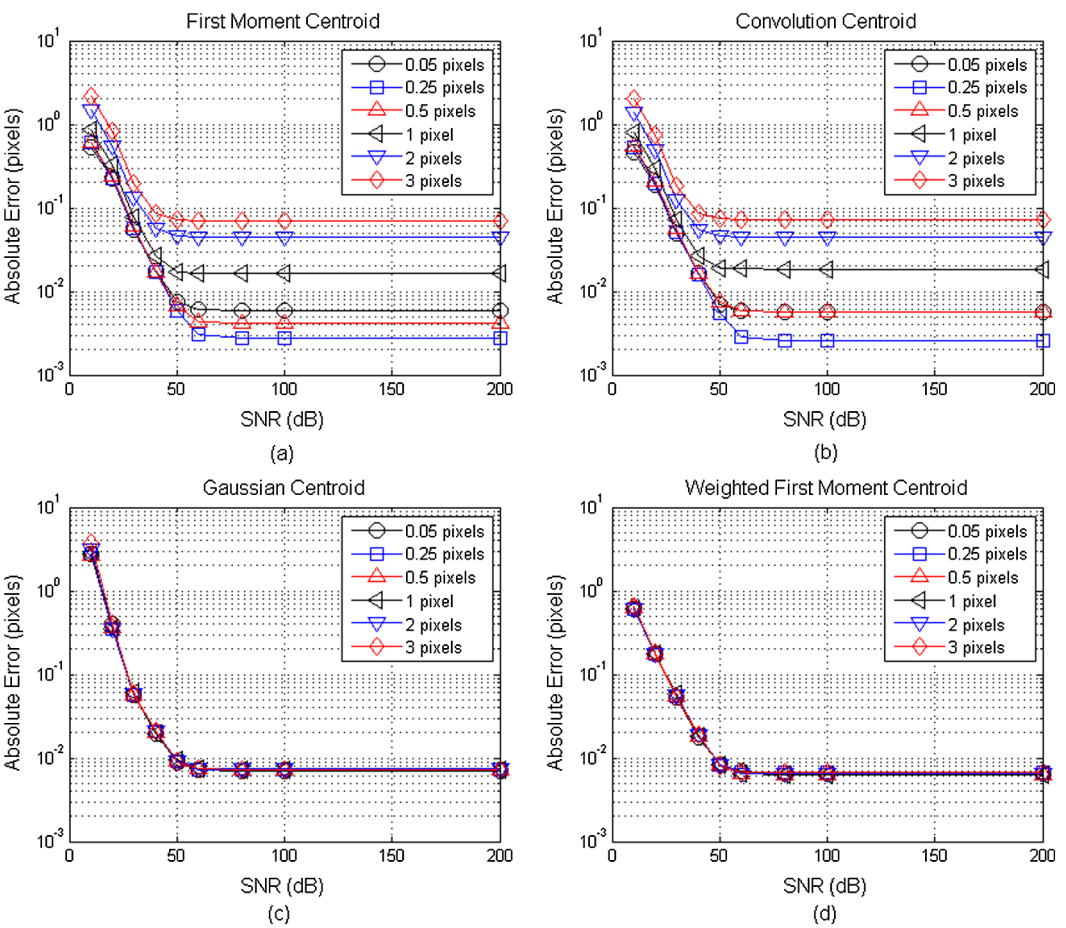

Fig. 13 Absolute error (pixels) versus SNR (dB) given six different spot positions with respect to the center of the AOI with a mean noise level of 0.025 after applying a 2nd order gamma correction. Error was computed based on four centroiding methods: (a) first moment, (b) convolution, (c) Gaussian, and (d) weighted first moment.

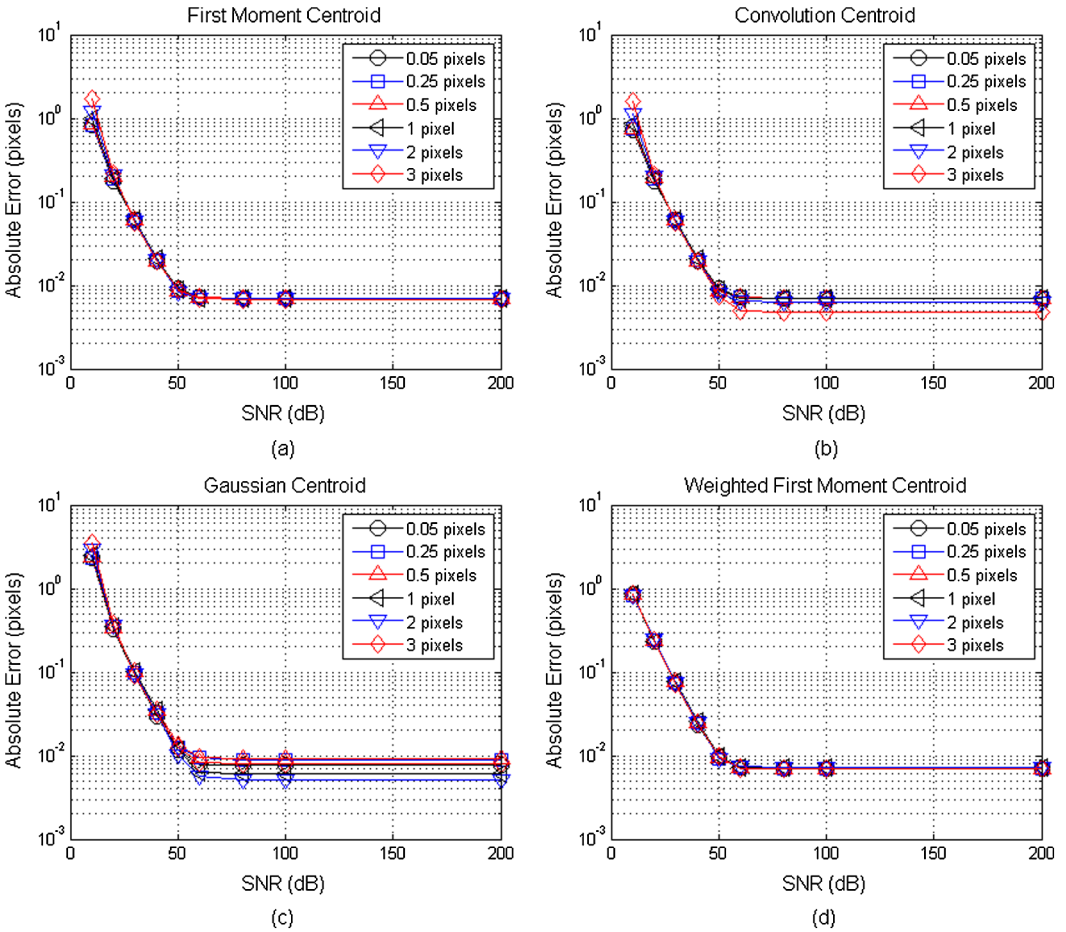

Fig. 14 Absolute error (pixels) versus SNR (dB) given six different spot positions with respect to the center of the AOI with a mean noise level of 0.025 after applying a 4th order gamma correction. Error was computed based on four centroiding methods: (a) first moment, (b) convolution, (c) Gaussian, and (d) weighted first moment.

decreases when a threshold percentage is applied to the image. Figure 16 shows the number of iterations required to reach convergence for the weighted first moment centroid versus percent threshold. At a SNR of 20, the number of iterations declines from approximately 12 to 6 as the percent threshold increases from 0% to 35%. Similar trends in the reduction of convergence iterations were observed at SNRs between 20 and 40. For each SNR, there exists a percent threshold which will essentially remove the majority of the background noise creating an image with the least number of iterations required to reach convergence. This threshold value decreases proportionally with decreasing mean noise level. At the lowest noise levels, corresponding to SNRs of 50 or more, a 5% threshold value reduces the number of required iterations to below four at which point no further improvement is seen.

4.3 *Windowing*

The effects of creating a window around the spot are also studied. In each simulation, the position of the pixel with the maximum intensity is determined. A window is created to isolate the relevant pixels centered at that maximum pixel location. All pixel values outside the windowed area are set equal to zero. Spot centers are estimated using the four centroiding methods on the redefined AOI pixels. Window sizes between 1 and 10 were simulated, where window size is defined as the $\pm$ distance in pixels from the center pixel within the window to each of the four window edges. For example, a window size shown on the graph of ± 1 refers to a window area of 9 pixels (3 pixels by 3 pixels) centered on the maximum pixel. Note that a window size of ± 10 does not change the image, given a 15×15 pixel AOI if the simulated spot remains within 3 pixels of the center of the AOI. Figure 17 shows absolute error (pixels) versus window size given a mean noise level of 0.025. For SNRs between 30 and 60, a window size of approximately ± 4 pixels produces the best results when applying the first moment, convolution, and Gaussian centroids. A slightly smaller window is required when the SNR drops to 20 and below. Similar to thresholding, the weighted first moment centroid does not benefit from windowing. Furthermore, window sizes of ± 4 or less, in which the outer portion of the spot becomes clipped by the window, actually reduces the accuracy of the weighted first moment's spot estimation. In other words, when the window size is smaller than the spot's FWHM the centroid estimation based on the weighted first moment method becomes corrupted.

The effect of windowing on the number of iterations required to reach convergence for the weighted first moment centroid was also examined. Figure 18 shows the number of iterations required to reach convergence versus window size for the weighted first moment centroid given a mean noise

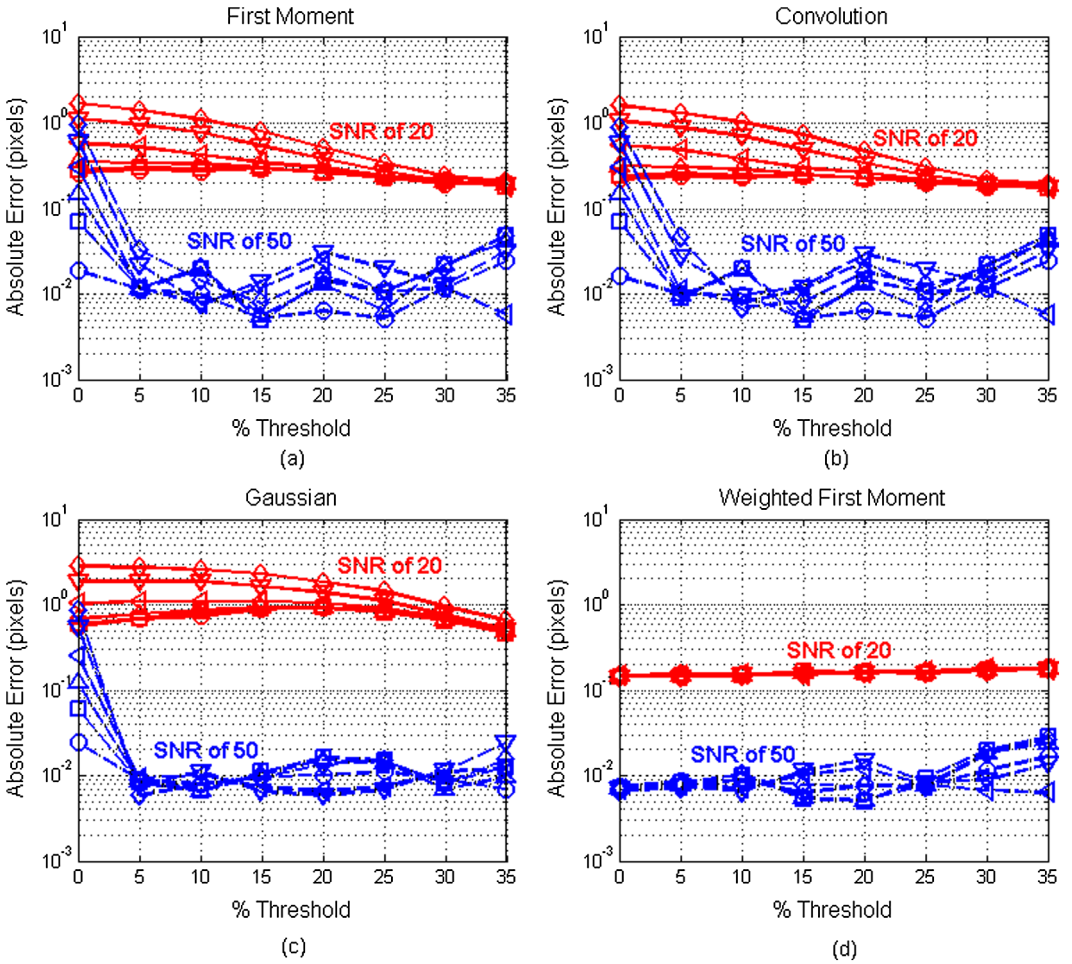

Fig. 15 Absolute error (pixels) versus percent threshold (%) given a mean noise level of approximately 0.025 at SNRs of 50 (dashed lines) and 20 (solid lines). Absolute error was computed at five different spot locations with respect to the AOI center (0.05: circle, 0.25: square, 0.5: upward-pointing triangle, 1: left-pointing triangle, and 2: downward-pointing triangle) using four centroiding methods: (a) first moment, (b) convolution, (c) Gaussian, and (d) weighted first moment.

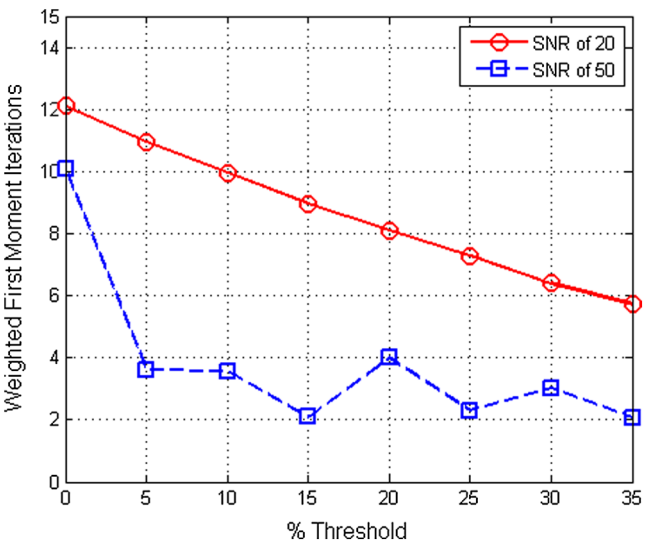

Fig. 16 Weighted first moment iterations required to reach convergence versus percent threshold given a mean noise level of 0.025 at two different SNR levels.

level of 0.025 and a spot position approximately 1 pixel from the AOI center. At SNRs above 30, a window size of ± 4 pixels slightly reduces the number of iterations required. However, when the SNR reduces to 20 or below, the only significant reduction in iterations occurs when the window size is reduced to ± 1 pixel. When taken into account with the absolute error results shown in Fig. 17(d), it is clear that creating a window this small around the spot results in increased error when computing spot position.

5 Image Features Effects

5.1 *Image Rotation*

There are a few different types of rotation that affect wavefront reconstruction accuracy including misalignment between the Shack-Hartmann sensor and the lenslet array, beam rotation, and rotation of a single spot. This section addresses centroid error induced by spot rotation which occurs when the outer lobes of the double sinc function are no longer aligned vertically and horizontally with the pixels. Typical spot rotation observed within the AAOL data sets are less than a degree. This section explores the effect that spot rotation plays on centroiding accuracy. A spot positioned

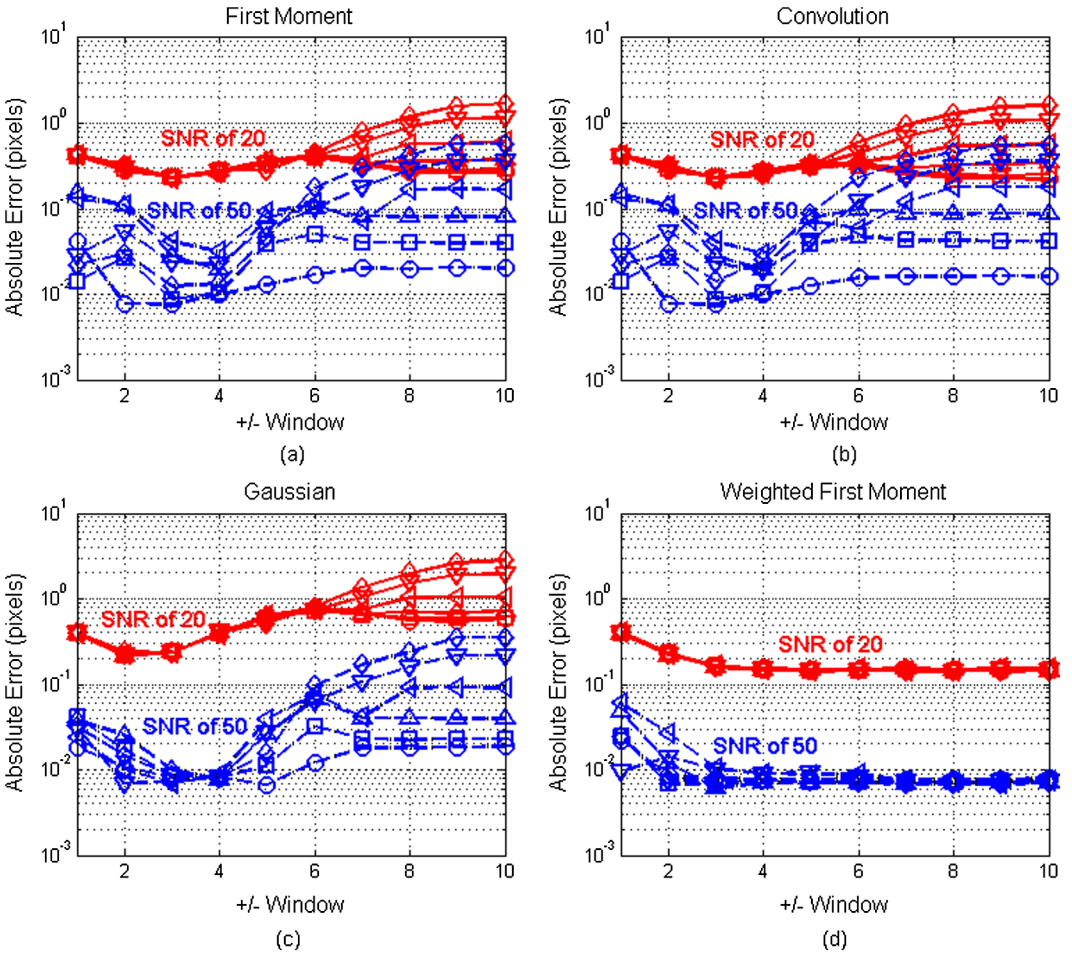

Fig. 17 Absolute error (pixels) versus window size (± pixels) given a mean noise level of approximately 0.025 at SNRs of 50 (dashed lines) and 20 (solid lines). Absolute error was computed at five different spot locations with respect to the AOI center (0.05: circle, 0.25: square, 0.5: upward-pointing triangle, 1: left-pointing triangle, and 2: downward-pointing triangle) using four centroiding methods: (a) first moment, (b) convolution, (c) Gaussian, and (d) weighted first moment.

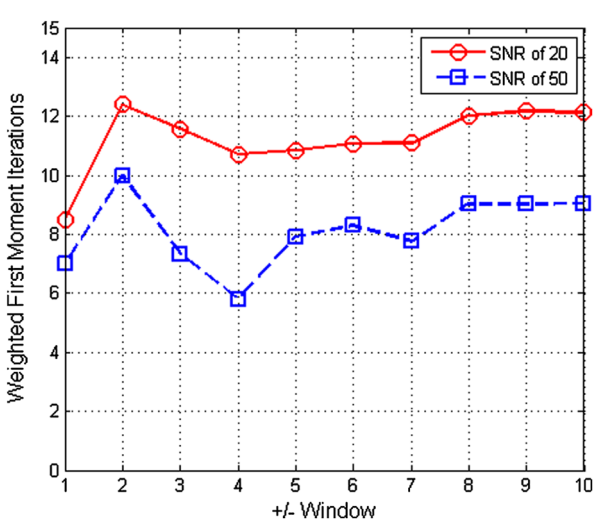

Fig. 18 Weighted first moment iterations required to reach convergence versus ± window size given a mean noise level of 0.025 at two different SNR levels.

approximately 1 pixel away from the AOI center was simulated within a 15×15 pixel area. Additive nonzero mean Gaussian noise was applied to the image after which the spot was rotated by a specified angle about the AOI center. As mentioned before, the rotation angle for the AAOL wavefront sensor was less than a degree but, purely for illustrative purposes, rotation angles including 0 deg, 0.25 deg, 0.5 deg, 1 deg, 2 deg, and 4 deg were simulated. Spot centers were estimated using each of the four different centroiding methods given the range of rotation angles. A second set of simulations was run given a 4th order gamma correction. Figure 19 shows absolute error versus SNR over the range of rotation angles listed above given a spot displaced approximately 1 pixel away from the AOI center. While this range of rotation angles has little to no effect on the accuracy of the first moment, convolution, and Gaussian centroids, the weighted first moment centroid experiences significant increases in error as the spot rotation increases. Once the spot rotation exceeds approximately 5 deg, the weighted first moment no longer outperforms the other three methods, however this amount of spot rotation is extremely rare. When a 4th order gamma correction is applied, spot rotation affects

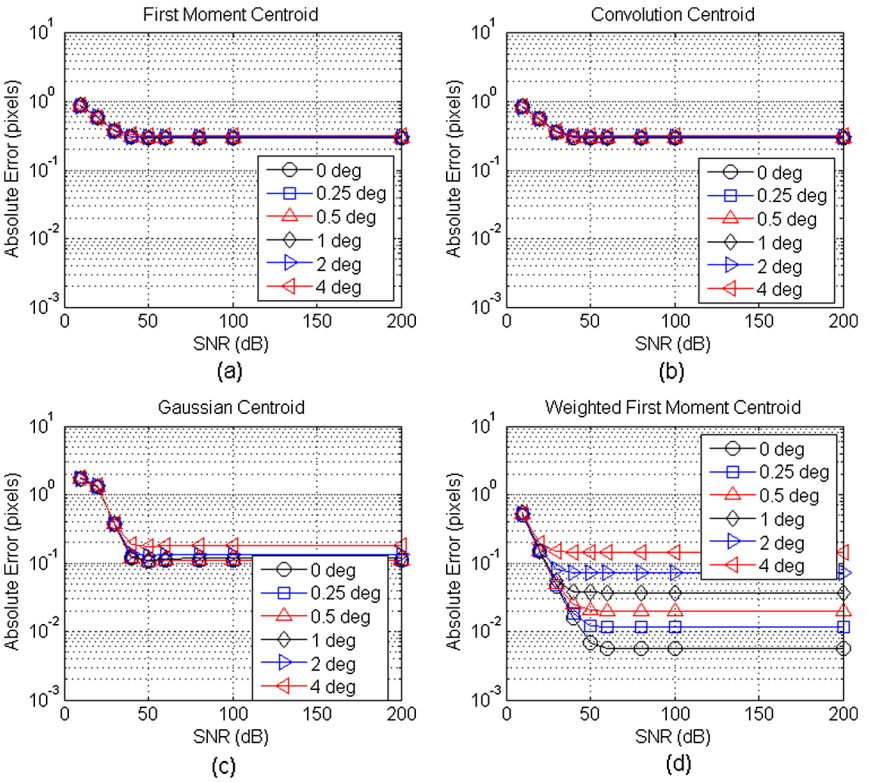

Fig. 19 Absolute error (pixels) versus SNR (dB) over a range of rotation angles given a mean noise level of 0.025. Error was computed based on four centroiding methods: (a) first moment, (b) convolution, (c) Gaussian, and (d) weighted first moment.

each centroiding method similarly, resulting in increased error with increased rotation as shown in Fig. 20. When the rotation angle exceeds approximately 3 deg, the gamma correction no longer provides any discernible improvement to the centroiding accuracy when comparing these results with Fig. 19.

5.2 *Spot Size*

The spot size or resolution of each spot also has an effect on centroiding accuracy. A range of spot sizes, defined by the approximate number of pixels measured across the spot's FWHM, are studied. Centroids were simulated using each of the four centroiding techniques with and without a 4th order gamma correction. Figure 21 shows absolute error versus SNR for each of the four centroiding methods given a range of spot sizes. The first moment and convolution centroids experience only small decreases in centroiding accuracy as the spot size decreases, while the Gaussian centroid is greatly affected by spot size losing any estimation advantage once the spot's FWHM reduces to approximately 3 pixels or less. The weighted first moment centroid does not show any appreciable decrease in absolute error until the spot size is reduced to a FWHM of approximately 1 pixel or less. Figure 22 shows similar results given a 4th order gamma correction. Overall, the gamma correction improves the accuracy of each centroiding method except for the weighted first moment as reported above in Sec. 4.1. It is interesting to note when comparing Fig. 21 to Fig. 22, that as the spot's FWHM is reduced to 2 pixels or less, the 4th order gamma correction actually has a negative effect on the weighted first moment's estimate of the spot center. At this spot size, the first moment centroid with 4th order gamma correction outperforms the weighted first moment.

6 Centroiding Results Applied to AAOL Flight Data

The simulation results presented above clearly show that the weighted first moment centroid consistently provides the most accurate spot center estimations. However, its accuracy is accompanied by significantly longer computational times in comparison to the first moment centroid calculation. It has also been shown that applying a 4th order gamma correction prior to computing the commonly used first moment centroid significantly reduces the amount of absolute error. The result is a spot center estimate similar to that found by the weighted first moment method, but with significantly less computational time. These two approaches, along with the thresholded first moment centroid (the method currently used to process the AAOL flight data), are applied to a series of 3000 AAOL Shack-Hartmann images. Wavefront statistics are computed and compared in an effort to visualize and quantify the effect of applying the "more-accurate" centroiding methods.

Individual wavefronts are reconstructed from the slopes which are inferred from the spot displacements obtained using the common first moment method and two "more-accurate" methods, the weighted first moment and the first moment centroid with 4th order gamma correction. Wavefront statistics are computed and a histogram of the temporal distribution of OPD_{RMS} values is created for each case, where OPD_{RMS} refers to the instantaneous spatial RMS of the OPD over the aperture. The first AAOL data set analyzed

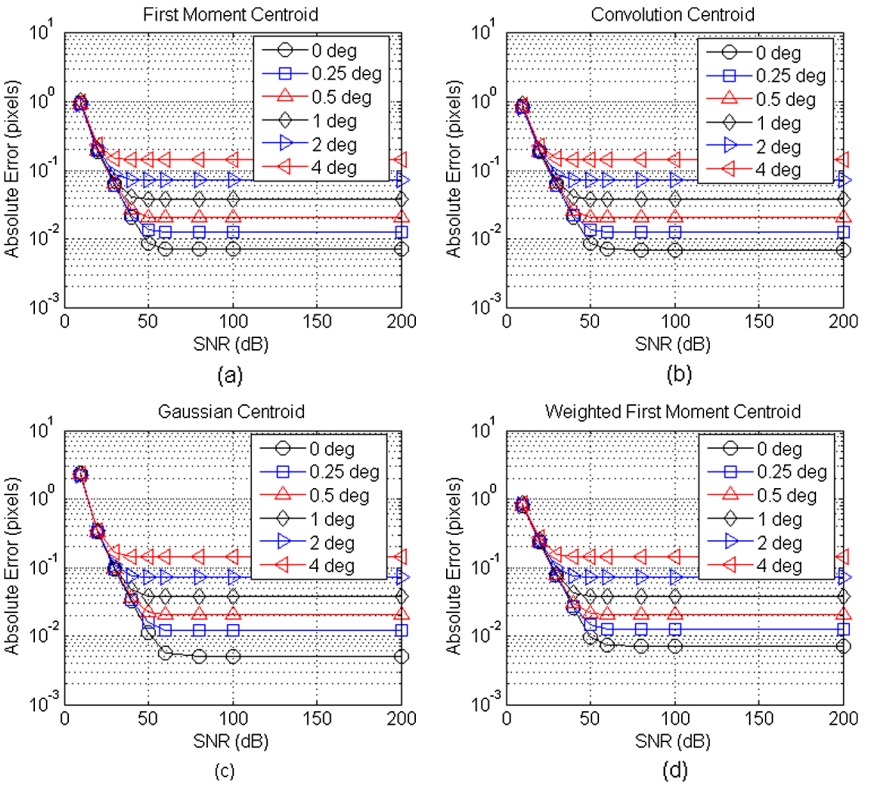

Fig. 20 Absolute error (pixels) versus SNR (dB) over a range of rotation angles given a mean noise level of 0.025 after applying a 4th order gamma correction. Error was computed based on four centroiding methods: (a) first moment, (b) convolution, (c) Gaussian, and (d) weighted first moment.

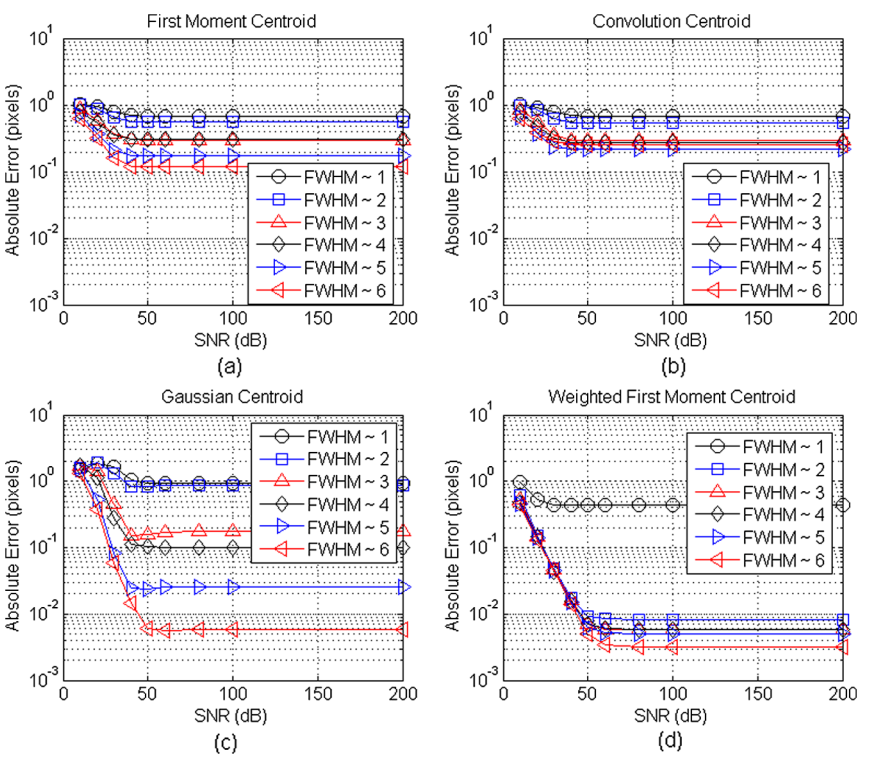

Fig. 21 Absolute error (pixels) versus SNR (dB) for a range of spot sizes given a mean noise level of 0.025. Error was computed based on four centroiding methods: (a) first moment, (b) convolution, (c) Gaussian, and (d) weighted first moment.

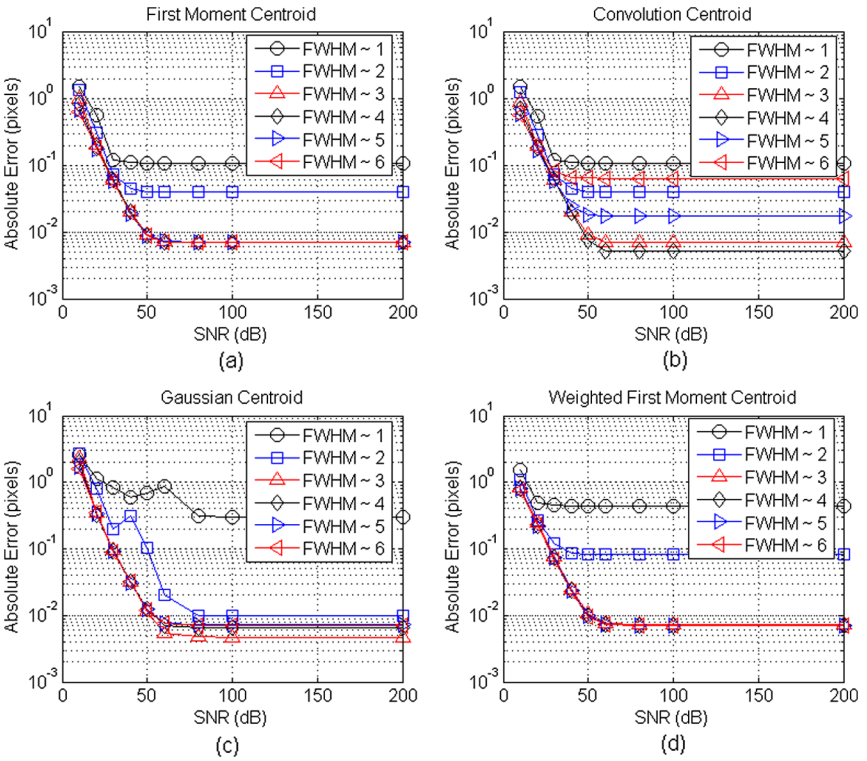

Fig. 22 Absolute error (pixels) versus SNR (dB) for a range of spot sizes given a mean noise level of 0.025 after applying a 4th order gamma correction. Error was computed based on four centroiding methods: (a) first moment, (b) convolution, (c) gaussian, and (d) weighted first moment.

below contains repeated images containing regions of spots with extremely low intensity levels in addition to individual spots that experience varying amounts of distortion. When images contain *problem areas* with low light levels and/or spot distortions, the resulting wavefront may become corrupted. This can cause significant discrepancies in spatial OPD across the aperture and consequently in the instantaneous OPD_{RMS} values. As a result, this may produce some outliers on a typically log-normal distribution of the time series of instantaneous OPD_{RMS}, representing a potential indication that the data may be flawed.[8] Figure 23 shows an individual Shack-Hartmann image from the set of AAOL flight data analyzed here. Four different AOIs are highlighted on the image, three of which may be considered problem areas with low light levels or spot distortion, while the fourth could be considered a good spot.

Figures 24–27 show expanded views of the highlighted AOIs from Fig. 23. In each figure the AOI is shown on the left and a further blown up image of the spot is shown on the right. Spot centers estimated using the first moment centroid with a 15% threshold (commonly used to process the AAOL data currently) are shown by a circle. The weighted first moment centroid is shown by a triangle and the first moment centroid with a 4th order gamma correction is shown by a square. While the true spot centers are unknown for this set of real data, these images are meant to provide a visual comparison of centroiding methods when applied to the AAOL flight data. Figure 24 is an example of a "good" spot where each of the three centroiding methods produce virtually identical estimates of the spot center. Figures 25 to 27 represent AOIs containing "poor" spots. In each of these figures the first moment with gamma correction and

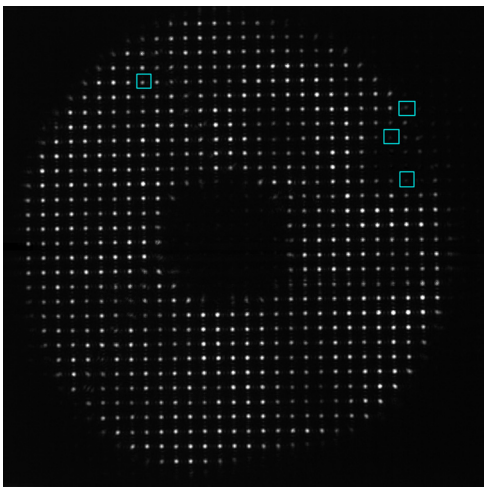

Fig. 23 Shack-Hartmann wavefront sensor image with four individual AOIs highlighted by boxes.

the weighted first moment centroids appear to be closer to the spot center than the first moment centroid.

Wavefronts were reconstructed from the array of spot displacements using the Southwell method[13] based on each of the three centroiding/image processing methods examined in this section. Note that tip/tilt has also been removed from the wavefront images shown below. Figure 28 shows individual reconstructed wavefronts corresponding to the Shack-Hartmann image depicted above in Fig. 23. The wavefront shown in Fig. 28(a) has been reconstructed based on the slopes inferred from the first moment centroid with 15%

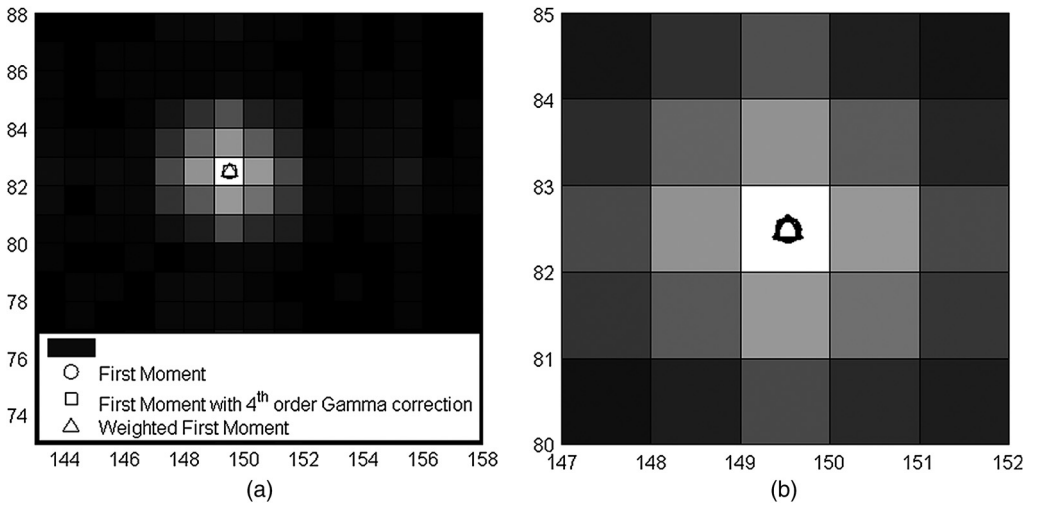

Fig. 24 (a) Expanded AOI and (b) blown-up view of spot corresponding to the upper left highlighted box in Fig. 23 showing three different spot center estimates.

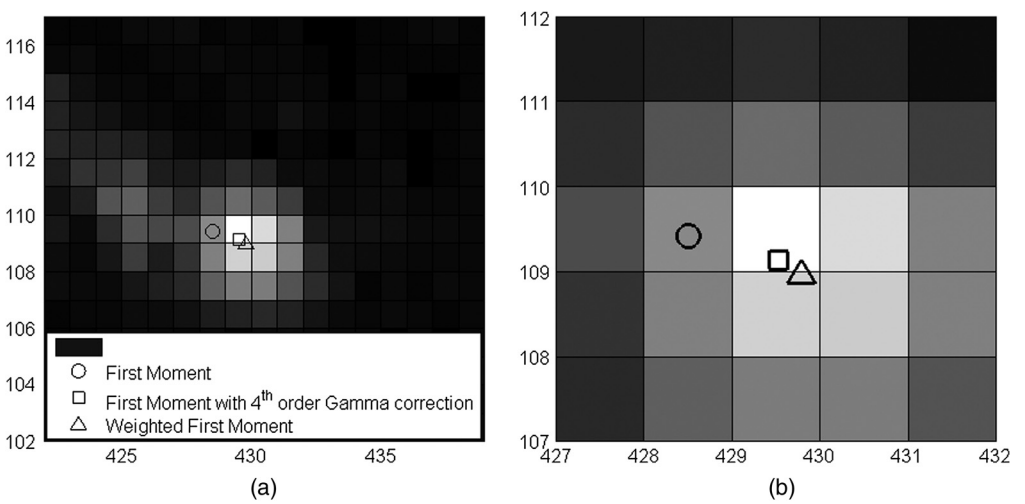

Fig. 25 (a) Expanded AOI and (b) blown-up view of spot corresponding to the upper right highlighted box in Fig. 23 showing three different spot center estimates.

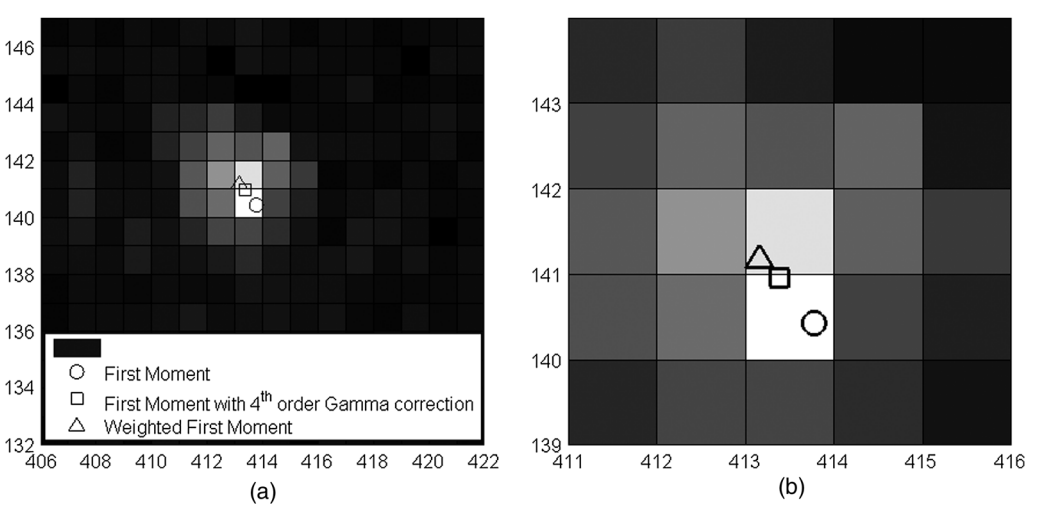

Fig. 26 (a) Expanded AOI and (b) blown-up view of spot corresponding to the middle right highlighted box in Fig. 23 showing three different spot center estimates.

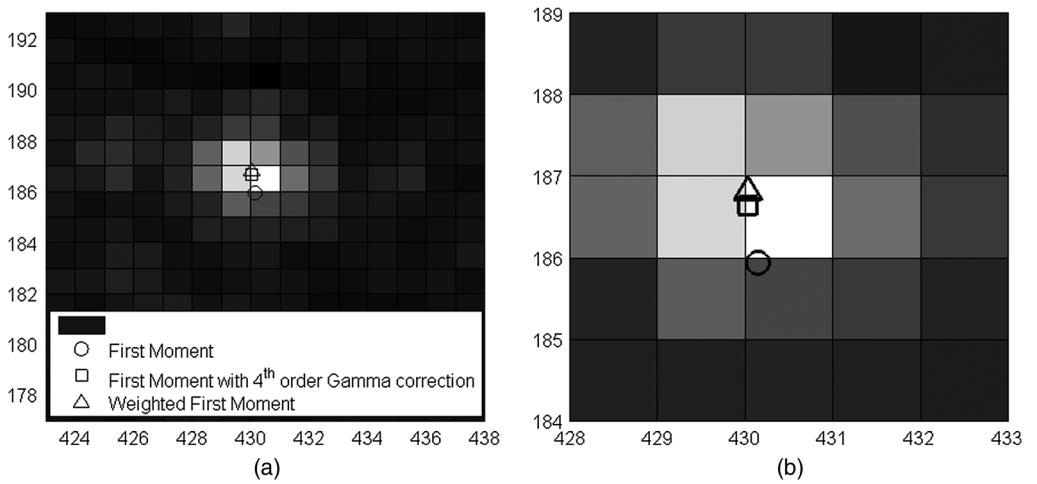

Fig. 27 (a) Expanded AOI and (b) blown-up view of spot corresponding to the lower right highlighted box in Fig. 23 showing three different spot center estimates.

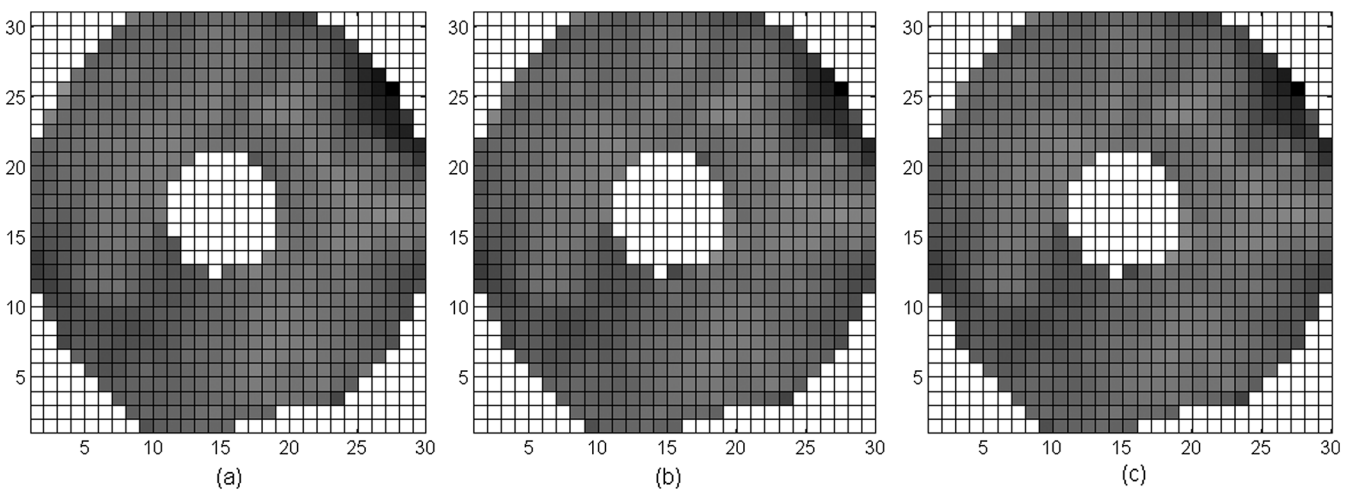

Fig. 28 Individual wavefront (microns) corresponding to the Shack-Hartmann image shown in Fig. 23 reconstructed from spot displacements estimated by (a) a first moment centroid with a 15% threshold, (b) a first moment centroid with a 4th order gamma correction, and (c) a weighted first moment centroid.

threshold spot displacements. Figure 28(b) shows the wavefront reconstructed based on spot displacements computed using the first moment centroid with 4th order gamma correction. And Fig. 28(c) similarly shows the reconstructed wavefront from the set of weighted first moment spot displacements. The dark area on the upper right corner of the wavefronts appears to be a corrupted area containing inaccuracies corresponding to the low intensity region on the Shack-Hartmann image pictured in Fig. 23. The wavefronts reconstructed from both the first moment centroids with 4th order gamma correction and the weighted first moment centroids appear to be less corrupted. A visual inspection of the results shown in Figs. 24–28 seem to indicate that when either of the "more-accurate" centroiding methods are applied to a set of real Shack-Hartmann images such as the AAOL flight data, little to no change is seen in the reconstructed wavefront if the spots are well-focused with a somewhat symmetric shape. However, improvements to the reconstructed wavefront can be expected in regions where the light intensity is low or the spots have become misshapen on the Shack-Hartmann image. This conclusion is supported by the following statistical AAOL results.

Wavefront statistics were computed to compare the effects that the three centroiding techniques have on the reconstructed wavefronts. A series of 3000 Shack-Hartmann images was analyzed for two different AAOL data sets. The first set of data, which corresponds to the results shown above in Figs. 24–28, contains multiple Shack-Hartmann images (similar to Fig. 23) with low light levels and individual spots that may be difficult to discern. This AAOL flight data could be considered a "poor" data set. The second set of AAOL flight data examined could be labeled a "good" data set in which the light levels remain fairly constant and the spots are consistently bright and symmetric. Individual wavefronts were reconstructed for both sets of data based upon spot displacements computed from each of the three different centroiding techniques described in this section: first moment with 15% threshold, first moment with 4th order gamma correction, and the weighted first moment. Spatially averaged OPD_{RMS} values were computed at an

instant in time for each series of wavefronts. In order to gain a better appreciation for the time series of wavefronts reconstructed based upon these three centroiding approaches, probability distribution functions of instantaneous OPD_{RMS} were plotted. Figure 29 shows histograms of OPD_{RMS} resulting from each of the three centroiding techniques for the "poor" AAOL data set. As shown by the circled area in Fig. 29(a), the thresholded first moment centroid produces an extended tail on the histogram indicating the presence of several larger OPD_{RMS} values within the time series of analyzed images. Outliers such as these are often an indication of erroneous wavefronts. As shown in Fig. 29(b) and 29(c), when using either of the "more-accurate" centroiding methods, the tail diminishes reducing the number of outliers. In addition, the standard deviation of the probability distribution decreases. These notable differences seem to indicate that the first moment centroid with 4th order gamma correction and the weighted first moment centroid improve the accuracy of the reconstructed wavefronts. The similarity between the mean OPD_{RMS} and their standard deviations

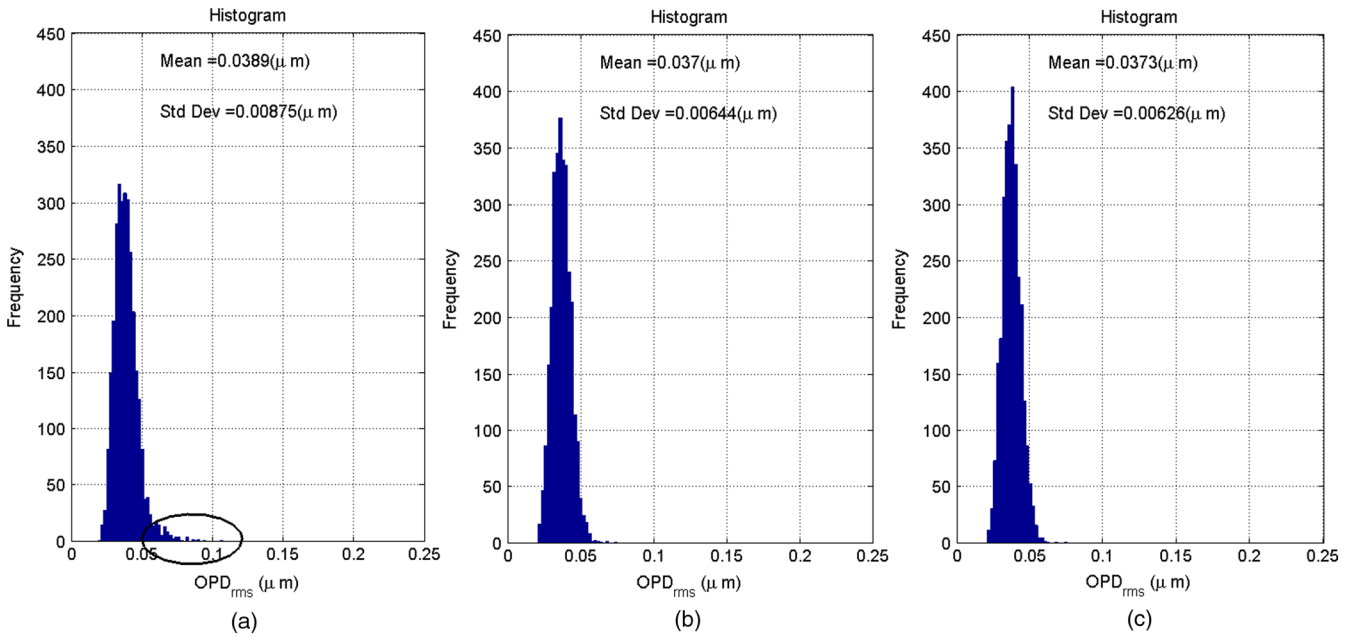

Fig. 29 Probability distribution functions of OPD_{RMS} computed from a set of "poor" AAOL data where the wavefronts are reconstructed based on spot displacements estimated using (a) a first moment centroid with a 15% threshold, (b) a first moment centroid with 4th order gamma correction, and (c) a weighted first moment centroid.

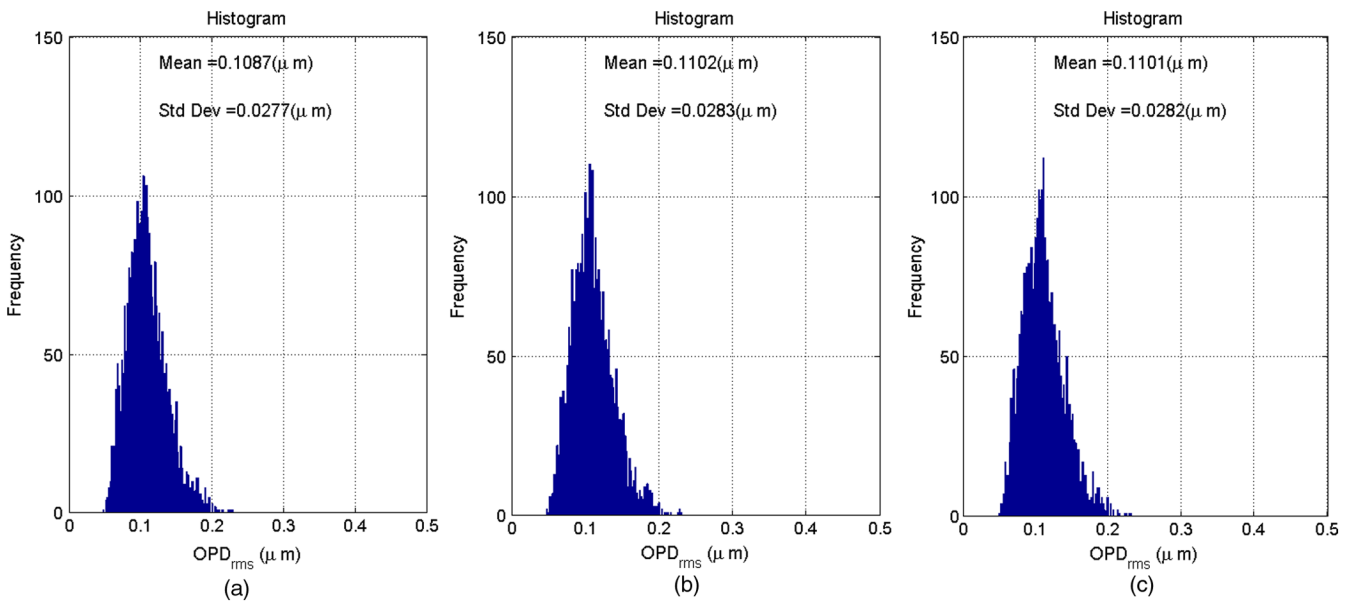

Fig. 30 Probability distribution functions of OPD_{RMS} computed from a set of "good" AAOL data where the wavefronts are reconstructed based on spot displacements estimated using (a) a first moment centroid with a 15% threshold, (b) a first moment centroid with 4th order gamma correction, and (c) a weighted first moment centroid.

for the "more-accurate" centroiding methods further validates these results. The overall difference in the reconstructed wavefront statistics when applying either of the "more-accurate" centroiding methods is a reduction in outlying OPD_{RMS} values (which was probably the result of several individual wavefronts containing significant error) and a reduction in the mean OPD_{RMS} from approximately 0.0389 to 0.037 μm. Figure 30 shows histograms of OPD_{RMS} computed from a "good" set of AAOL data. As evident from the distribution the wavefronts in this data set contain a wider range of aberrations. However, the overall shape of each histogram is extremely similar and the mean OPD_{RMS} increases only slightly from approximately 0.109 to 0.11 μm. Therefore, when the spots shown on the Shack-Hartmann images are consistently bright and symmetric there appears to be no appreciable change in the wavefront statistics.

Overall, the visually more accurate spot center estimates shown in Figs. 24–27, the reduction in the wavefronts problem area shown in Fig. 28, and the reduction in outliers present in the probability distribution of instantaneous OPD_{RMS} values shown in Fig. 29, seem to indicate that the first moment centroid with a 4th order gamma correction and the weighted first moment centroid provides a more accurate spot center estimate which produces more accurate wavefront statistics. The only appreciable difference between these two methods is the increased computational time taken by the weighted first moment. While the increased accuracy of "more-accurate" centroiding methods compared to the method currently being used to process the AAOL data may not alter the time-averaged statistics significantly in all cases, it would affect the spatial content of instantaneous wavefronts; accuracy of which is important when characterizing aero-optic effects using methods such as proper orthogonal decomposition.[14]

7 Conclusions

The ability to accurately locate the centers of an array of Shack-Hartmann spots is critical when characterizing aero-optic effects and studying mitigation techniques. The accuracy of the centroiding method currently being used to process the AAOL data is compared with three other methods. In addition, a few different image processing techniques and their effect on spot center estimation are examined. The centroiding methods studied here include, the currently used first moment centroid, a convolution centroid, a Gaussian centroid, and a weighted first moment centroid. A double sinc function was used to simulate a spot pattern similar to those seen in the AAOL data on a 15×15 pixel image. Varying degrees of additive nonzero mean Gaussian noise were applied. Spot estimations based on each of the four centroiding methods were compared to the spots true center. The weighted first moment centroid was shown to estimate the spot center with the most accuracy independent of spot position within the AOI, while the other methods exhibit increased error as the spot moves away from the image center due to their intensity based computations. However, the weighted first moment centroid's iterative approach takes significantly more computational time compared to the commonly used first moment calculation.

Three additional image-processing techniques were studied. Second and fourth order gamma corrections, thresholding, and windowing were applied to the simulated image prior to computing each of the four centroids. Absolute error was compared. Thresholding and windowing were shown to increase the accuracy of the first three methods while displaying optimal ranges which varied slightly with mean noise level. The 4th order gamma correction provided the most improvement, reducing absolute error of the commonly used first moment centroid to that of the weighted first moment centroid given low to moderate mean noise levels. Finally, the two "most-accurate" centroiding methods (first moment with 4th order gamma correction and weighted first moment) were applied to two different sets of AAOL flight data along with the centroiding method used currently to process the data. Wavefronts were reconstructed based on each method and wavefront statistics were compared. Increased accuracy was illustrated by visual inspection of several individual AOIs within an AAOL Shack-Hartmann image. Seemingly flawed wavefront distortions were also shown to reduce when using the "more-accurate" centroiding methods. And finally, a reduction in the outlying probability distribution tail for the instantaneous OPD_{RMS} computed from a series of AAOL Shack-Hartmann wavefront images further shows the benefit of using either of the "more-accurate" centroiding methods described in this paper.

Acknowledgments

This work was funded by the High Energy Laser-Multidisciplinary Research Initiative (HEL-MRI FY07) Airborne Aero-Optics Laboratory (AAOL) and administered through the Air Force Office for Scientific Research under grant number FA9550-07-1-0574. The US government is authorized to reproduce and distribute reprints for government purposes notwithstanding any copyright notation thereon. The authors are grateful to the reviewer's for their recommendations and suggestions improving the overall content of this paper.

References

1. E. J. Fitzgerald and E. J. Jumper, "The optical distortion mechanism in a nearly incompressible free shear layer," *J. Fluid Mech.* **512**, 153–189 (2004).
2. R. M. Rennie, D. A. Duffin, and E. J. Jumper, "Characterization and aero-optic correction of a forced two-dimensional weakly compressible shear layer," *AIAA J.* **46**(11), 2787–2795 (2008).
3. S. Godeyev and E. J. Jumper, "Fluid dynamics and aero-optics of turrets," *Progr. Aero. Sci.*, **46**(8), 388–400 (2010).
4. S. Gordeyev, T. Hayden, and E. J. Jumper, "Aero-optical and flow measurements over a flat-windowed turret," *AIAA J.* **45**(2), 347–357, (2007).
5. B. Platt and R. Shack, "History and principles of Shack-Hartmann wavefront sensing," *J. Refract. Surg.* **17**(5), 573–577, (2001).
6. C. Porter et al., "Flight measurements of aero-optical distortions from a flat-windowed turret on the Airborne Aero-Optics Laboratory (AAOL)," in *42nd AIAA Plasmadynamics and Lasers Conference*, paper 2011–3280, AIAA, Honolulu, HA (2011).
7. E. J. Jumper et al., "The Airborne Aero-Optics Laboratory," *Proc. SPIE* **8395**, 839507 (2012).
8. N. De Lucca, S. Gordeyev, and E. J. Jumper, "The Airborne Aero-Optics Laboratory, recent data," *Proc. SPIE* **8395**, 839508 (2012).
9. I. T. Young, J. J. Gerbrands, and L. J. van Vliet, Section 3.5 in *Fundamentals of Image Processing*, pp. 13–19, Delft University of Technology, Netherlands (1998).
10. S. M. Anthony and S. Granick, "Image analysis with rapid and accurate two-dimensional Gaussian fitting," *Langmuir* **25**(14), 8152–8160 (2009).
11. A. Vyas, M. B. Roopashree, and B. R. Prasad, "Optimization of existing centroiding algorithms for Shack Hartmann sensor," in *Proc. National Conference on Innovative Computational Intelligence & Security Systems*, pp. 400–405, Sona College of Technology, Salem (2009).
12. R. Maini and H. Aggarwal, "A comprehensive review of image enhancement techniques," *J. Comput.* **2**(3), 8–13 (2010).

13. S. I. Panagopoulou and D. R. Neal, "Zonal matrix iterative method for wavefront reconstruction from gradient measurements," *J. Refract. Sur.* **21**(5), S563–S569 (2005).
14. D. J. Goorskey, R. Drye, and M. R. Whiteley, "Spatial and temporal characterization of AAOL flight test data," *Proc. SPIE* **8395**, 839509 (2012).

Alice M. Nightingale received her BS in mechanical engineering in 2003 from Lake Superior State University, MI. She received her MS in 2007 in aerospace and mechanical engineering from the University of Notre Dame, IN. She completed her PhD in 2011 in aerospace and mechanical engineering at the University of Notre Dame, IN, specializing in aero-optics and controls. She is currently a research assistant faculty at the University of Notre Dame, focusing on aero-optics and image processing.

Stanislav Gordeyev is a research associate professor at Department of Aerospace and Mechanical Engineering, University of Notre Dame. He is an internationally recognized expert in investigating optical distortions caused by compressible turbulent flows around airborne systems. His expertise includes performing complex experimental investigations of optical aberrations, both in time-averaged and instantaneous sense, in boundary layers, shear layers and wakes, as well as around complex geometries, like side-mounted turrets at subsonic and transonic speeds; experimental results and developed models are currently widely used to design laser airborne systems, as well to validate computational codes to predict optical distortions caused by turbulent flows. He is also actively involved in various studies of different mitigation techniques to improve the overall optical performance of airborne systems.